TOPICAL REVIEW • OPEN ACCESS

Distribution (function) of relaxation times, successor to complex nonlinear least squares analysis of electrochemical impedance spectroscopy?

View the article online for updates and enhancements.

Journal of Physics: Energy

TOPICAL REVIEW

Distribution (function) of relaxation times, successor to complex nonlinear least squares analysis of electrochemical impedance spectroscopy?

Bernard A Boukamp

University of Twente, Fac. of Science and Technology & MESA+ Institute for Nanotechnology, P.O. Box 217, Enschede, AE 7500 The Netherlands

E-mail: b.a.boukamp@utwente.nl

Abstract

Electrochemical impedance spectroscopy (EIS) and complex nonlinear least squares (CNLS) analysis with an equivalent circuit (EqC) has been the standard research tool in Solid State Electrochemistry for many decades. With an ever increasing interest in the development of energy related materials with complex structures, the impedance spectra are becoming too complex for a simple CNLS-analysis. Inversion of the data from the frequency domain to a distribution function of relaxation times (DFRT), i.e. the τ-domain, has shown to present a better separation and visualization of the underlying electrochemical processes. These are presented by peaks with characteristic time constants that are associated with the separate processes. Hence, the interest in EIS-analysis with inversion to a DFRT has rapidly gained attention over the last decennia. In this contribution a brief review of the applications and limitations of the DFRT procedure is presented. Some examples from the field of solid oxide fuel cells (SOFC) and Li-ion based battery research are discussed. When possible a comparison is made between the exact DFRT (derived from known DFRT expressions) and three inversion methods: Fourier Transform (FT), Tikhonov Regularization and a recently developed multi-(RQ) CNLS-fit: 'm(RQ)fit'. It is shown that the three differently derived DFRT's can differ significantly, while the impedances reconstructed from the DFRT with the inverse process show a quite good match with the original data.

1. Introduction

Electrochemical impedance spectroscopy (EIS) is a very important research tool in the field of energy related materials and systems, e.g. fuel cells, batteries and super capacitors. It is often used for the characterization of materials and identification of charge transport and transfer processes, and charge storage in electrode systems, but also for following effects of aging and degradation. The first applications of EIS were performed in systems with liquid electrolytes, studying electrode processes at (mostly) inert electrodes, notably Sluyters and Sluyters-Rehbach have made significant contributions to its development [1, 2]. In the seventies of the last century EIS was introduced into solid state electrochemistry, replacing the up till then used single frequency practice. The data analysis of these, mostly simple, systems was often done graphically, but a more robust computer assisted analysis with fitting procedures was soon introduced. Several computer programs, based on a complex nonlinear least squares (CNLS) algorithm, were developed for fitting an equivalent circuit (EqC) model to a data set, e.g. Wapenaar and Schoonman [3], Macdonald and Potter (LEVM) [4], Boukamp (EquivCrt) [5, 6] and Dygas *et al* [7].

As research progressed, the studied systems became more complex. Finding an appropriate EqC was no longer a straightforward process. EquivCrt [6] and its Windows successor, EqCwin [8], offered the advantage of de-convoluting the impedance spectra by partial fits and subsequent subtractions, either in series or in parallel, of recognized partial contributions, see [9, 10] for examples. Such a procedure yields a possible EqC model as well as reasonable starting values for the fit parameters in the final full CNLS-analysis

procedure [6]. A brief overview of the development in EIS has been presented in [9]. For a complete introduction into EIS a few good books are available, notably by Barsoukov and Macdonald [11], Orazem and Tribolet [12], Lovich [13] and Lasia [14].

An often heard criticism of CNLS impedance analysis is that the choice of an EqC could be rather ambiguous. It is true that different EqC's can have exactly identical impedance responses. Fletcher [15] has compiled a list of these, so-called, degenerate EqC's. Besides this list of circuits with identical frequency dispersions, there is also the possibility that, within the experimental error, two unrelated circuits can yield almost similar impedance graphs. The important point, however, is that the chosen EqC must have physical meaning in relation with the experimental cell. Another point of concern is the possibility of 'over parameterization', although this can often be seen in the appearance of large relative errors for some parameters in the CNLS-analysis results. Too many parameters can also lead to 'rejection' by the CNLS-fit, i.e. values become either very small (a short) or very large (open circuit). Some CNLS-analysis programs can automatically find a possible EqC (e.g. Zview© from Scribner Associates [16]), however, these results should be interpreted with caution. In a comparative study on a porous $Ca_3Co_4O_{9+\delta}$ cathode, Rolle *et al* found that the partial fit and subtraction method resulted in a significantly better analysis with a more appropriate EqC [17].

Electrodes of solid oxide fuel cells (SOFC) and solid oxide electrolyzer cells (SOEC) have a porous structure, often composed of two, or more, components. Impedance measurements are used to characterize the electrode properties, but the EqC's used in the CNLS-analysis provide just an approximate, global presentation of the actual electrochemical processes which are distributed over the microstructure. For an accurate modelling of the electrode properties it is essential to include the microstructure properties, such as porosity, tortuosity and grain size. An accurate 3D reconstruction of the microstructure can be achieved with a focused ion beam (FIB), cutting small slices of the electrode (at 40–50 nm apart) which are subsequently imaged with a scanning electron microscope (SEM) [18, 19]. The sequence of SEM images is used to reconstruct a discrete 3D model. Using finite element modeling (FEM) the electrode properties can then be simulated, provided that essential materials information (electronic and ionic conductivities, surface exchange rates, etc) is available. The FIB-FEM method has been successfully applied to modelling the properties of a nickel-yttria stabilized zirconia (Ni/YSZ) cermet anode [18, 19]. An excellent match was obtained between the simulated impedance, based on the 3D microstructure reconstruction and FEM modelling, and the actual measurement. The FIB-SEM method was also successfully used by Almar *et al* [20] for obtaining an accurate estimation of the porosity and tortuosity of two types of Perovskite electrodes. This information was used in the modelling of the electrode properties with the 'chemical impedance' model of Adler *et al* [21] and Lu *et al* [22]. The complexity of the FIB-SEM approach, however, makes this method not suited for general electrode characterizations with impedance analysis.

Because of these complications there has been a search for a 'model free' presentation of the time constants associated with the electrode and electrolyte processes. This can be achieved by transforming the impedance data to a distribution (function) of relaxation times (DRT, or DFRT). In this contribution the abbreviation DFRT will be used. Although the use of DFRT's has gotten notable attention over the last 10 to 15 years, it has already been applied in 1983 by Franklin and De Bruin [23] to give an alternative presentation of the impedance data of solid state electrolytes.

In this review a brief overview is presented of so-called inversion methods, with which a DFRT is obtained from impedance data. As for several dispersive elements (e.g. Havriliak-Negami, Gerischer, Finite Length Warburg or FLW) and simple circuits exact distribution functions exist, it is possible to compare in a number of cases the DFRT obtained by inversion methods with the exact representation of the distribution function based on an accurate EqC. The first section will show how the DFRT is obtained from an impedance data set. An overview of different inversion methods is given. Three of these will be used in further comparisons of specific cases.

The main considerations are: how unique and reliable are the DFRT's and can they give a complete picture of all dispersive processes that contribute to the measured impedance. Secondly: how much difference is there between the obtained DFRT's for the three presented methods and, when available, with the 'exact' DFRT derived from the CNLS-analysis. A number of examples from SOFC electrodes, lithium-ion batteries and special electrolyte/electrode systems will be presented. But also synthetic data will be analyzed to show the possibilities and limitations of the use of DFRT's. Equivalent Circuit models will be presented using the 'Circuit Description Code' (CDC) as developed by Boukamp [24].

2. Principle of the DFRT

A (RC) circuit is characterized by a single time constant, $\tau_{(RC)} = R \cdot C$. When the capacitance is replaced by a constant phase element (CPE: $Y_{CPE}(\omega) = Y_0 \cdot (j\omega)^{\varphi}$, Brug *et al* [25]), as often is observed in real

experiments, then the time constant shows a distribution in the τ-domain (i.e. the inverse of the frequency domain, $\tau = \omega^{-1}$) with $\tau_{max} = (R{\cdot}Y_0)^{1/\varphi}$. This distribution can be made visible in a τ-domain plot of the DFRT, $G(\tau)$. This distribution function is derived from the impedance through solving a 'Fredholm integral of the second kind':

$$Z(\omega_i) = R_\infty + R_p \int_0^\infty \frac{\gamma(\tau)}{1 + j\omega_i\tau}\,d\tau = R_\infty + R_p \int_{-\infty}^\infty \frac{G(\tau)}{1 + j\omega_i\tau}\,d\ln\tau \tag{1}$$

Here R_p is the polarization resistance ($R_p = R_{dc} - R_{f\text{-max}}$) and $G(\tau) = \tau \cdot \gamma(\tau)$, with

$$\int_{-\infty}^\infty G(\tau)\,d\ln\tau = 1 \tag{2}$$

The second representation in equation (1) with $G(\tau)$ is to be preferred as the relaxation times are best presented on a logarithmic τ-axis. The Fredholm integral of equation (1) is known as an 'ill-posed inverse problem'. This means that very many solutions for $G(\tau)$ exist. But the requirement that $G(\tau)$ must always be positive reduces the number of solutions considerably.

An example of an ***unrestricted*** transformation, using a discretized summation for equation (1), is the Kramers-Kronig data validation test procedure published in [26]. Here a series connection of parallel (RC) circuits was fitted to the impedance data. The predefined time constants, $\tau_k = R_k.C_k$ were logarithmically spaced with seven τ-values per decade, with $\tau_{min} = (\omega_{max})^{-1}$ and $\tau_{max} = (\omega_{min})^{-1}$. Solving the following relation for all R_k only required a single matrix inversion, resulting in a set of R_k values ($k = 1 \dots M$):

$$Z(\omega_i) = R_\infty + \sum_{k=1}^M R_k \frac{1}{1 + j\omega_i\tau_k} \tag{3}$$

The KK-test showed an excellent fit for high quality impedance data. The simulated impedance dispersion was smooth between data points. The distribution in the R_k values, however, was almost alternating positive and negative (see figures 5 and 6 in [26]), thus far-removed from providing a usable distribution of time constants.

While the (RC) combination is represented by a δ-function in the τ-domain, the (RQ) combination shows a symmetric, bell-shaped, curve in the τ-domain. The exact expression (which will be derived further down) is given by:

$$R \cdot G(\tau) = \frac{R\sin(\varphi\pi)}{2\pi\left(\cosh\left[\varphi\ln\left(\frac{\tau_0}{\tau}\right)\right] + \cos(\varphi\pi)\right)} \tag{4}$$

with $\tau_0 = (R \cdot Y_0)^{1/\varphi}$. The shape strongly depends on the frequency exponent, φ. Figure 1 shows as an example the DFRT for a (RQ) circuit with a value of $\varphi = 0.9$. The δ-function for a (RC), i.e. $\varphi = 1$, is also shown.

2.1. Methods of inversion

There are quite a number of inversion methods for equation (1). The group of Ivers-Tiffée have used for a long time a Fast Fourier Transform method (FFT), [27, 28]. For this they used the imaginary part of the impedance, which requires that the data is properly Kramers-Kronig transformable [26]:

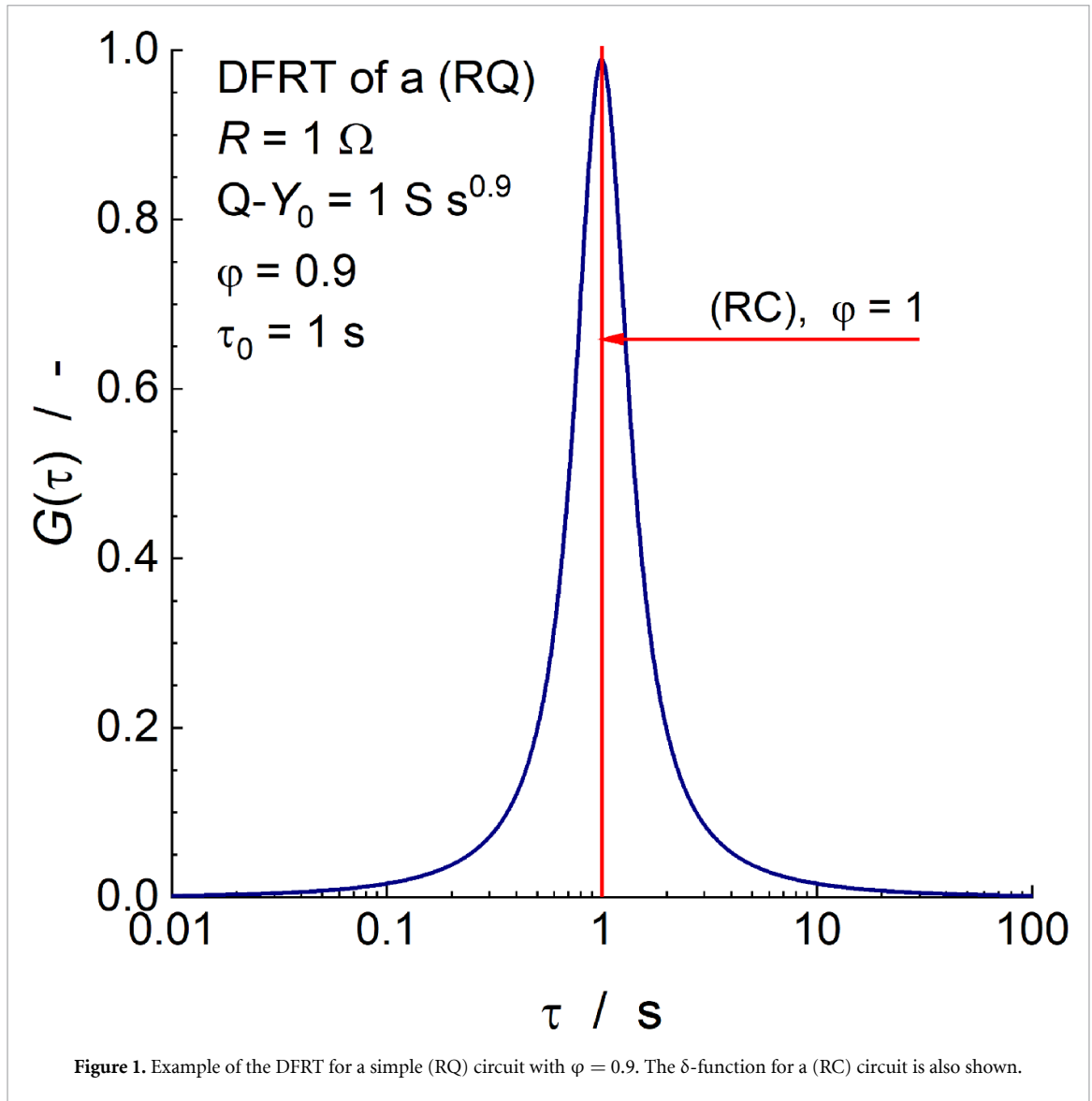$$Z_{im}(\omega_i) = R_p \int_0^\infty \frac{-\omega_i\tau}{1 + \omega_i^2\tau^2}\gamma(\tau)\,d\tau \tag{5}$$

Inserting new variables with: $x = \ln\left(\frac{\omega}{\omega_0}\right)$, $y = \ln(\omega\tau)$ and $g(y - x) = \tau \cdot \gamma(\tau)$, leads to:

$$Z_{im}(\omega_i) = -\frac{R_p}{2}\int_{-\infty}^\infty \operatorname{sech}(y) \cdot g(y - x)\,dy \tag{6}$$

Discretizing and performing the first Fourier Transform (FT) to de-convolute the integral of equation (6) results in:

$$\tilde{Z}_{im}(p) = -NT\frac{R_p}{2}\tilde{S}(p) \cdot \tilde{G}(p) \tag{7}$$

The tilde, '$\sim$', denotes the FT of the corresponding function, N is the number of data points, T is the sampling interval, with $T = (N-1)^{-1}\ln(\omega_{max}/\omega_{min})$. $\tilde{S}(p)$ is the Fourier transform of the sech(y) function.

Figure 1. Example of the DFRT for a simple (RQ) circuit with $\varphi = 0.9$. The δ-function for a (RC) circuit is also shown.
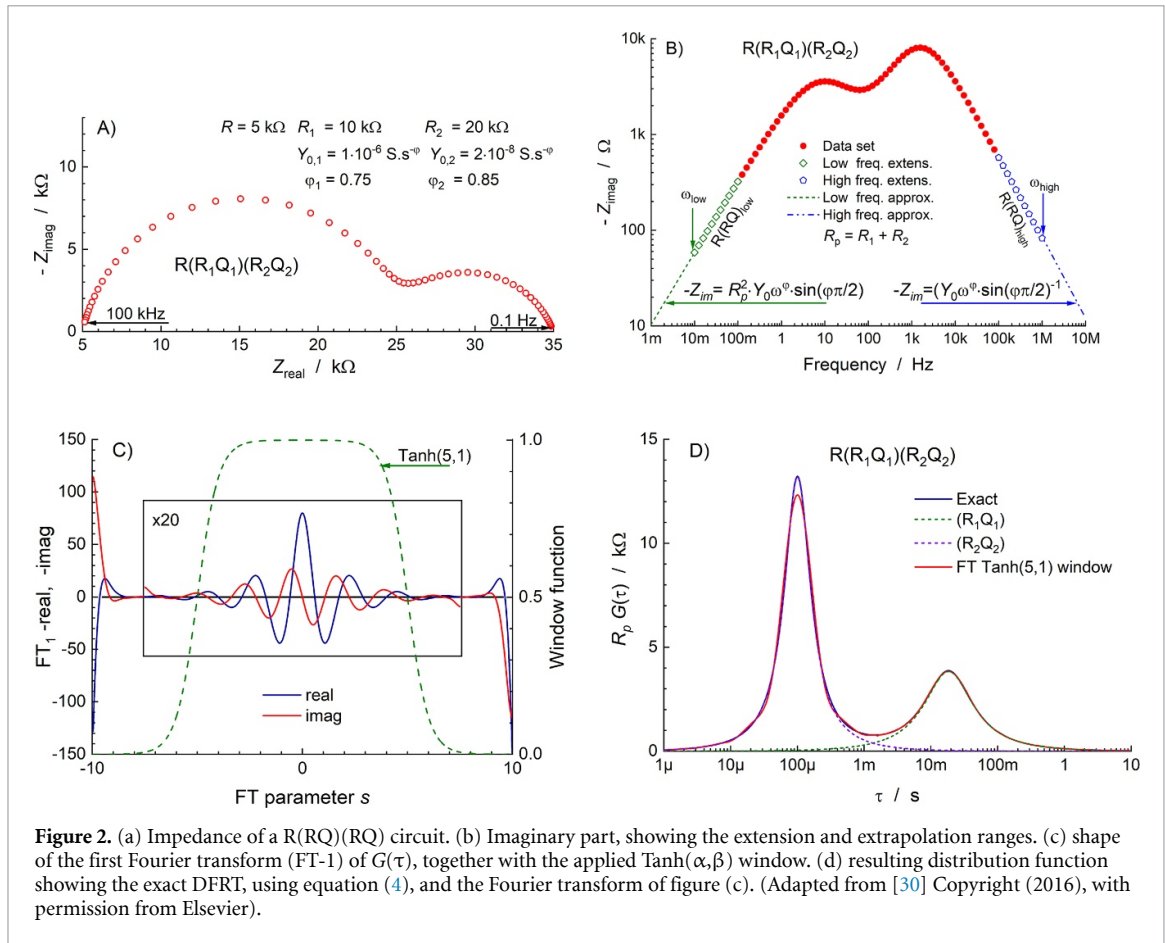
$G(\tau)$ can now be found by the inverse FT. But it is essential to apply a window function to the first FFT in order to remove strong oscillations in the end regions of p. This will be demonstrated further on with the use of an extended regular FT method [29, 30]. Hence, the shape and especially the width of this window function are important parameters that have significant influence on the appearance of the resulting distribution function, $G(\tau)$.

An alternative to the FFT was derived by the author in [29–31]. It was noted that quite often the end-regions of a measured dispersion could be extended with a simple R(RQ) circuit which was fitted to a selection of the end-region data points (about 5–10 data sets, depending on the fitting error). This could be used to extrapolate the dispersion to higher end lower frequencies. Above a certain frequency, ω_{high}, for the high-end extrapolation and below a frequency, ω_{low}, for the low-end extrapolation the FTs of the extrapolations can replaced by the respective ***analytical*** expressions:

$$Q_{hi} \int_{x_{hi}}^{\infty} e^{-\varphi x} \cdot e^{-jsx} dx = Q_{hi} \cdot e^{-\varphi x_{hi}} \left[\frac{\varphi \cos sx_{hi} - s \sin sx_{hi}}{s^2 + \varphi^2} - j\frac{s \cos sx_{hi} + \varphi \sin sx_{hi}}{s^2 + \varphi^2} \right]$$

$$Q_{lo} \int_{-\infty}^{x_{lo}} e^{\varphi x} \cdot e^{-jsx} dx = Q_{lo} \cdot e^{\varphi x_{lo}} \left[\frac{\varphi \cos sx_{lo} + s \sin sx_{lo}}{s^2 + \varphi^2} + j\frac{s \cos sx_{lo} - \varphi \sin sx_{lo}}{s^2 + \varphi^2} \right]$$

(8)

With: $x_{hi} = \ln \omega_{high}$, $x_{lo} = \ln \omega_{low}$, $Q_{hi} = Y_0^{-1} \cdot \sin(\varphi\pi/2)$ and $Q_{lo} = R^2 Y_0 \cdot \sin(\varphi\pi/2)$. The two sets of R, Y_0 and φ values are derived from the respective R(RQ) fits in both end regions (see [29] for details). This allows integration of the first FT, FT-1, from $-\infty$ to $+\infty$. Between ω_{low} and ω_{high} a simple discrete quadratic summation procedure was used. A full explanation is presented in [29, 30]. Despite this improvement over the FFT, which is only performed over a fixed frequency range and thus introducing 'end' errors, the first FT showed also significant oscillations in the end-regions, still requiring the use of a

Figure 2. (a) Impedance of a R(RQ)(RQ) circuit. (b) Imaginary part, showing the extension and extrapolation ranges. (c) shape of the first Fourier transform (FT-1) of $G(\tau)$, together with the applied $\text{Tanh}(\alpha,\beta)$ window. (d) resulting distribution function showing the exact DFRT, using equation (4), and the Fourier transform of figure (c). (Adapted from [30] Copyright (2016), with permission from Elsevier).

Window function. The standard window function, the Hann window, is based on a cosine function:

$$W(s) = \frac{1}{2}\left(1 + \cos\left(\frac{\pi s}{s_{max}}\right)\right), |s| \le s_{max} \text{ and } W(s) = 0, \; |s| \ge s_{max} \qquad (9)$$
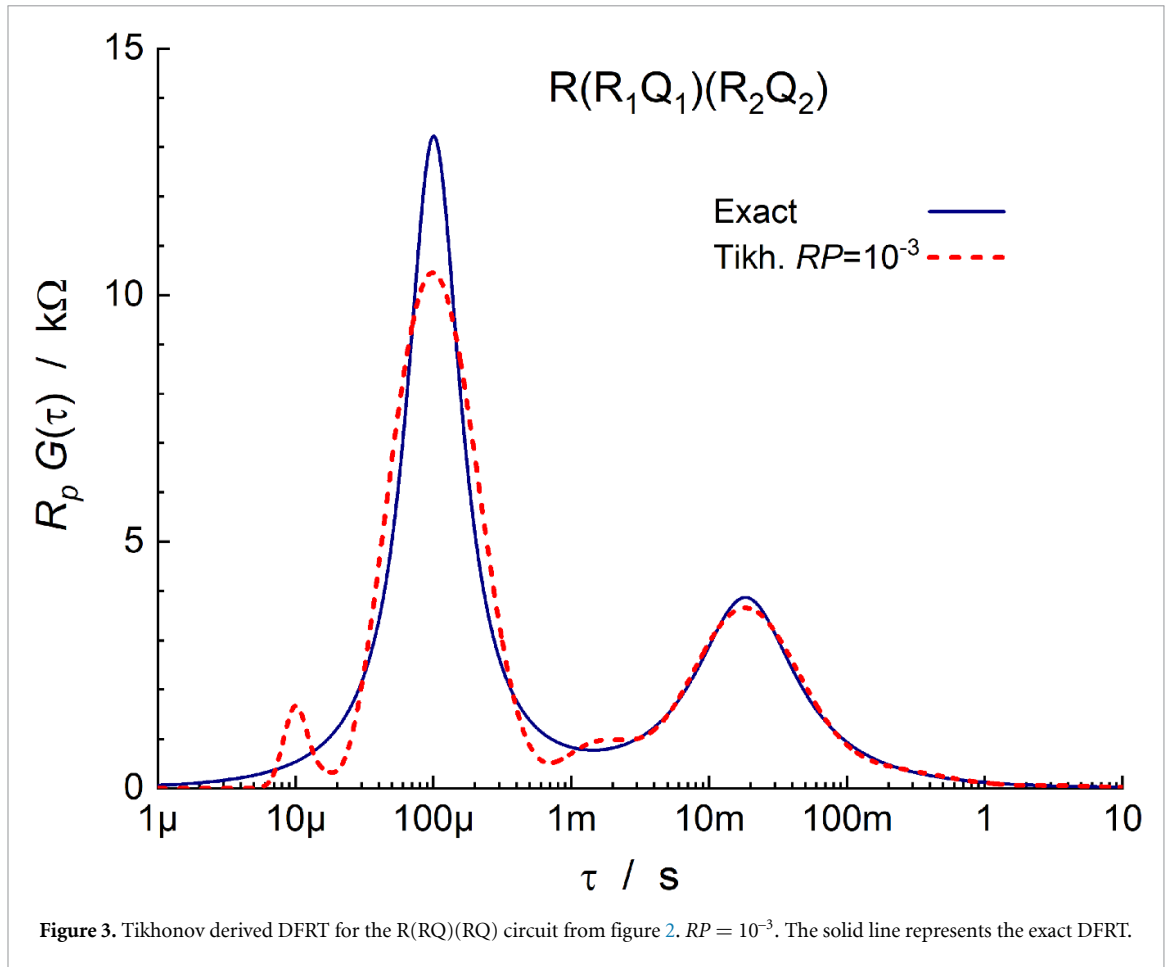
The window width is set by s_{max}. A large value of s_{max} will lead to unwanted oscillations, a too small value to a lowered and widened peak shape. An alternative approach was presented in [29] with a 'tanh' based window function:

$$W(s) = \frac{(\tanh\left[\beta\left(\alpha+s\right)\right]+1)(\tanh\left[\beta\left(\alpha-s\right)\right]+1)}{4} \qquad (10)$$

The advantage of this window is that a larger central part of the window function is close to 1 (leaving that part of FT-1 intact). The width (at half height) is set by the α parameter, the steepness of the window sides by β. Generally a value of $\beta \approx 1$ works well, lowering β leads to significant oscillations in $G(\tau)$ with a small period. Increasing β adds also some small oscillations with a rather large period. More significant is setting the α-value, this really depends on the quality of the data. There is no simple rule for setting α, apart from obtaining an 'acceptable' appearance of $G(\tau)$. In the following this window function will be presented as $\text{Tanh}(\alpha,\beta)$, e.g: $\text{Tanh}(5,1)$.

The application of the FT-methods is shown for a simple R(RQ)(RQ) circuit in figure 2 [30]. Figure 2(a) shows the impedance, figure 2(b) the extrapolation procedure in the $\log(f)$—$\log(-Z_{\text{imag}})$ plane, figure 2(c) shows the first Fourier transform, $\tilde{G}(\tau)$. The center part is 20 times enlarged to enhance visibility. The applied window function, $\text{Tanh}(5,1)$, is also shown. In figure 2(d) the resulting distribution function is compared with the exact DFRT, which is derived from equation (4)

Tikhonov Regularization is a procedure developed for solving ill-posed inversion problems and is used in a very broad field of applications. In 1994 Hansen presented a general Matlab® package for analysis and solution of discrete ill-posed problems [32–34]. Dion and Lasia have used this package to deconvolute impedance spectra of hydrogen adsorption on Pt electrodes [35]. The last 10 to 15 years have seen a significant increase in publications on Tikhonov Regularization procedures, specifically dedicated to impedance analysis [36–46]. This regularization method also requires the adjustment of a Regularization

Figure 3. Tikhonov derived DFRT for the R(RQ)(RQ) circuit from figure 2. $RP = 10^{-3}$. The solid line represents the exact DFRT.

Parameter, *RP*, in order to obtain an acceptable result. Wan [44] has written a user friendly MatLab® program, DRTtools [47], for impedance analysis. This software package is freely available from the internet. Figure 3 shows the DFRT of the R(RQ)(RQ) simulation of figure 2 with $RP = 10^{-3}$. The exact DFRT is also presented. A quite good match is obtained with some minor oscillations.
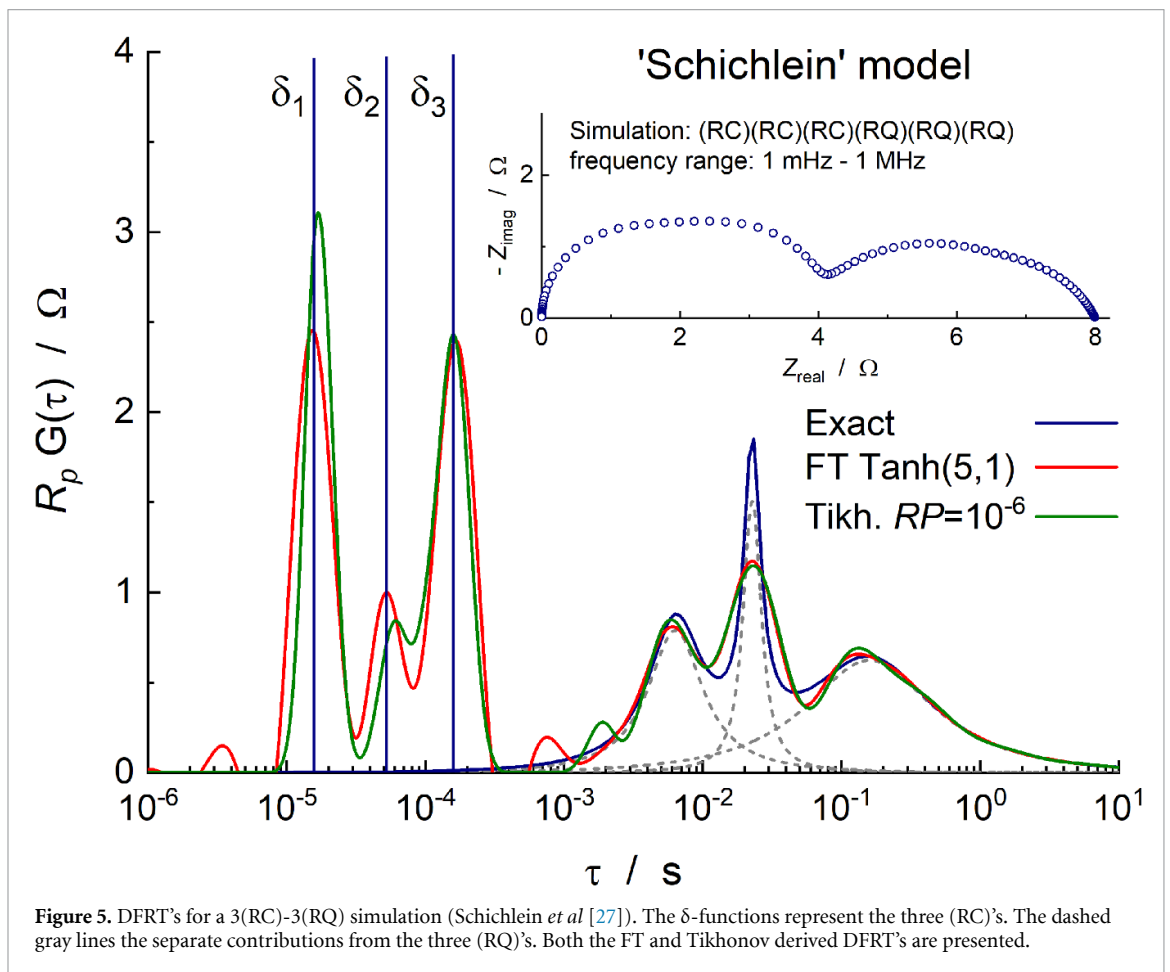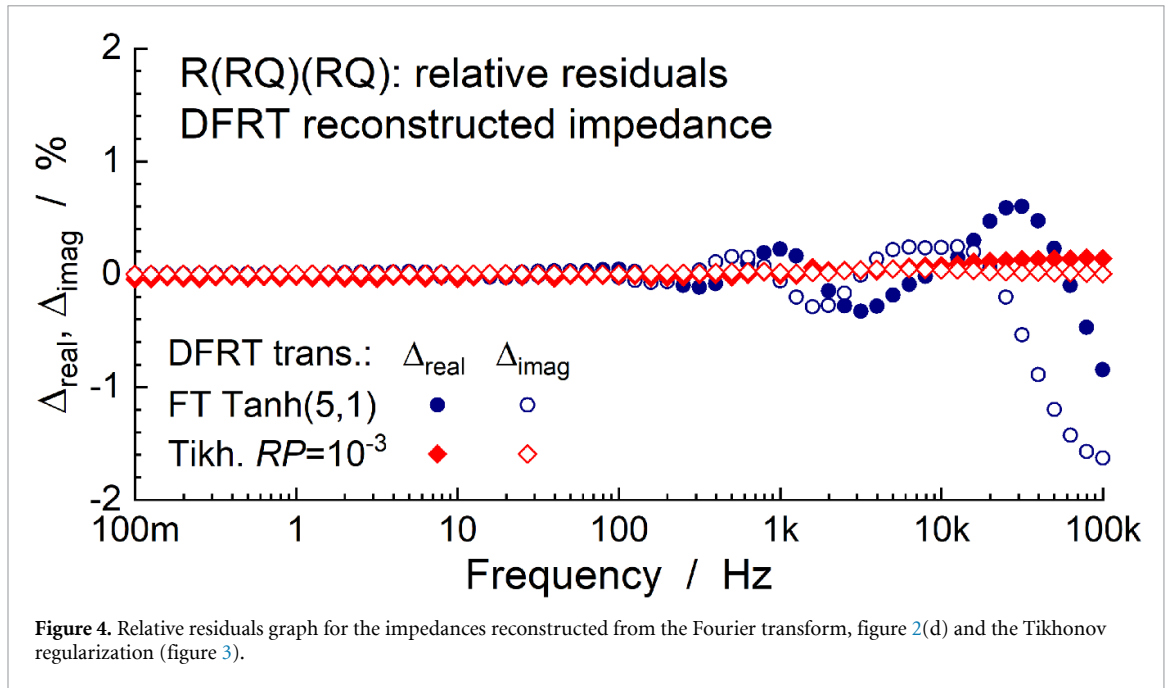
It is easy to inspect the quality (validity) of the obtained DFRT by using equation (1). With $G(\tau)$ known the impedance can be reconstructed using the integration. Deviations between the original data and the reconstructed data can best be presented in a so-called relative residuals graph, with:

$$\delta_{real}(\omega) = \frac{Z_{real}(\omega) - ZR_{real}(\omega)}{|Z(\omega)|}, \text{ and } \delta_{imag}(\omega) = \frac{Z_{imag}(\omega) - ZR_{imag}(\omega)}{|Z(\omega)|} \tag{11}$$

$ZR(\omega)$ represents the impedance values reconstructed from the DFRT. Figure 4 shows a compilation of the relative residuals for the Fourier transform of figure 2(d) and the Tikhonov inversion of figure 3. This figure presents a slight advantage for the FT with a general error level below 0.2%. The Tikhonov regularization shows deviations in the high frequency range.

Setting the *RP*-value is quite critical. Too small a value causes additional oscillations, increasing the *RP*-value lowers the peak height and widens the peak shape. This is demonstrated with the complex simulation used by Schichlein *et al* [27], see insert in figure 5. Direct CNLS-analysis of such a dispersion is quite complicated, however, the transformation to a DFRT clearly shows the different time constants that are present. Both the FT and the Tikhonov inversions show in figure 5 clearly marked peaks. Figure 6 shows the influence of the Tikhonov regularization parameter on the shape of the DFRT for the Schichlein simulation. It is clearly seen that with increasing *RP* the DFRT becomes more smooth, but is losing details, notably in the high frequency region where the three peaks (three (RC) δ-functions) reduce to two peaks. Despite this limitation, the Tikhonov inversion method is currently the most used procedure for obtaining a DFRT.

A different approach has been presented by Horlin, [48, 49]. He used the 'Max Entropy' method to obtain the DFRT's of impedance data, but again a smoothing parameter needs to be introduced in order to remove unwanted oscillations from the DFRT. This method has, however, not found many followers in the field of impedance analysis.

Figure 4. Relative residuals graph for the impedances reconstructed from the Fourier transform, figure 2(d) and the Tikhonov regularization (figure 3).

Figure 5. DFRT's for a 3(RC)-3(RQ) simulation (Schichlein *et al* [27]). The δ-functions represent the three (RC)'s. The dashed gray lines the separate contributions from the three (RQ)'s. Both the FT and Tikhonov derived DFRT's are presented.

The three methods presented above, FT, Tikhonov Regularization and Max Entropy, all require the adjustment of a 'smoothing parameter'. This enhances the chance that either extra peaks (oscillations) lead to misinterpretations or that small contributions to the DFRT are ignored. There are two methods that do not involve such a smoothing parameter.
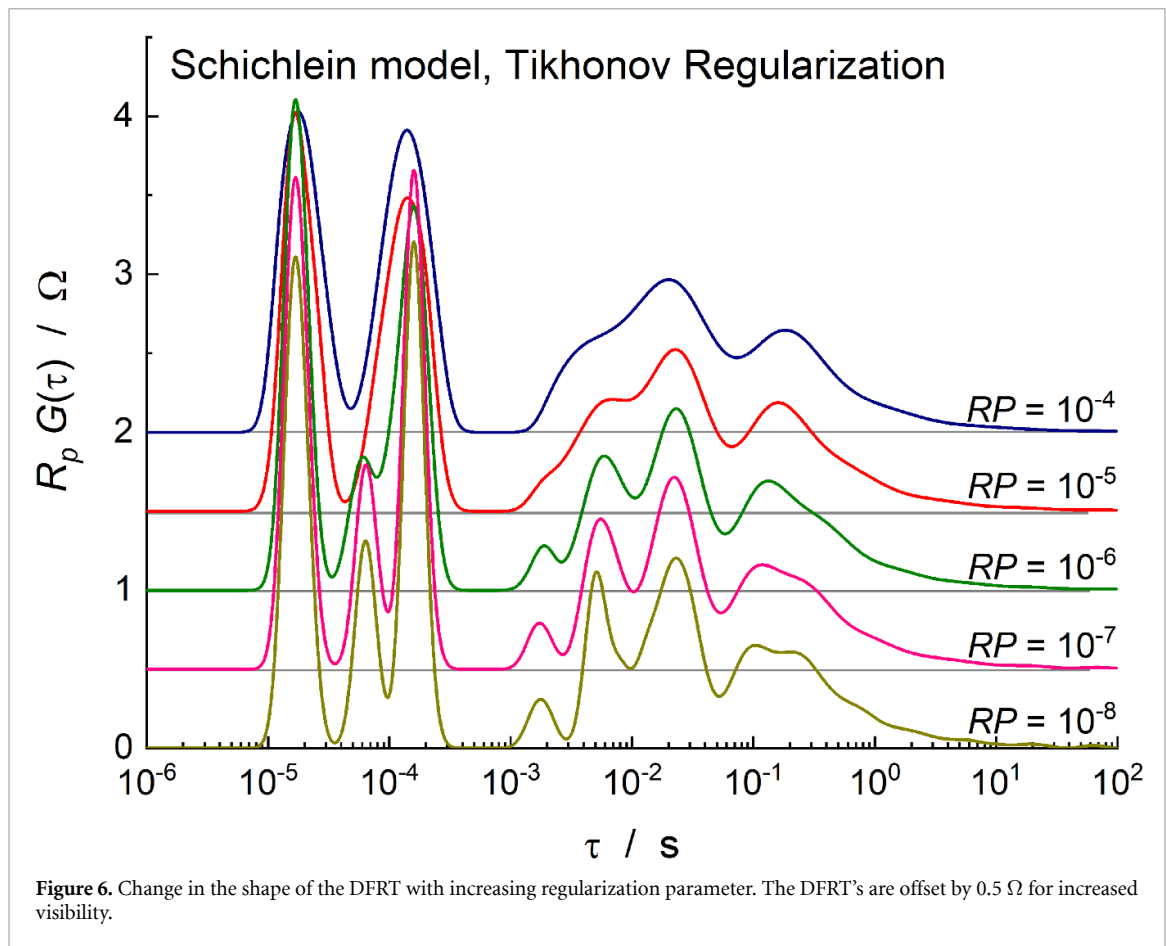
Figure 6. Change in the shape of the DFRT with increasing regularization parameter. The DFRT's are offset by 0.5 Ω for increased visibility.

2.2. Methods without adjustable parameter

In the group of Tsur a genetic algorithm method [50–53] has been developed for obtaining a DFRT directly from the impedance data. In this procedure, called Impedance Spectroscopy Genetic Programming, the ISGP program selects a number of distribution functions from a 'toolbox', with randomly generated parameter values (within realistic bounds) to form a large 'genetic pool'. The fitness of each 'parameter and function set' is calculated from the comparison of the reconstructed impedances with the actual measurement, using equation (1). From this large 'genetic pool' a selection is taken of function and parameter sets with the highest fitness score (lowest χ^2-value). With this selection a new generation is formed by cross-over of genes (parameter values) and random mutations. The procedure is continued until a predefined stopping criterium is met, e.g. a minimum χ^2-value is reached. To avoid over-parameterization a penalty for the number of parameters is included. The method seems to work well, although genetic algorithms can be quite time consuming. A more important issue is the selected distribution functions, these should at least have physical significance with respect to the charge transport and transfer processes in the electrochemical system under study.

The second method without a smoothing parameter has been derived by this author. It was observed that for rather complex impedances (e.g. porous electrodes in SOFC/SOEC research) these could be fitted with a series of (RQ) elements with very small residual errors [29, 30]. In this process the data is modeled with an increasing number of series connected (RQ) circuits until an optimal fit is obtained. This method has been named the m(RQ)fit. As for each (RQ) a DFRT can be calculated, the overall DFRT is the sum of the separate contributions. A minor problem is when a (RQ) with $\varphi = 1$ (i.e. a capacitance) appears. This results in a δ-function in the τ-domain. The use of a sharp Gauss function allows the contribution of a (RC) to be included in a graphical presentation of the DFRT [30]. This Gauss function is given by:

$$R \cdot G_{(RC)}(\tau) = \frac{R}{W\sqrt{\pi}} e^{-\left[\ln\left(\frac{\tau}{\tau_0}\right)/W\right]^2}$$ (12)

W is the width parameter, a value of $W = 0.15$ was found to give a good presentation in the τ-domain, while the error in the reconstructed impedance remains relatively small [30]. Unfortunately, the m(RQ)fit method cannot be applied in all cases, sometimes a negative $(\overline{RQ})$ arises, which is unwanted in the DFRT (for

a normal impedance). Examples of the m(RQ)fit method will be presented together with the FT and the Tikhonov Regularization (Tikh.) inversions.

3. Direct inversions

Quite often it is possible to find an EqC with a linear combination of well-known circuit elements, such as the parallel combination of a resistance and a CPE, (RQ) or Zarc, the Havriliak-Negami (H-N) response, the Gerischer (special case of the H-N response) or the finite length Warburg (FLW). For all these elements an exact representation in the τ-domain exist. The overall distribution function, $G(\tau)$, is then formed by the sum of the separate DFRT's:

$$R_p \cdot G(\tau) = \sum_i Z_{0,i} \cdot G_i(\tau), \text{with}: R_p = \sum_i Z_{0,i} \tag{13}$$

The exact representation can be derived from the impedance function by following the procedure described by Fuoss and Kirkwood [54]:

$$Z_0 \cdot G(\tau) = \frac{1}{\pi} \left[Z_{imag}\left(z + j\frac{\pi}{2}\right) + Z_{imag}\left(z - j\frac{\pi}{2}\right) \right] \tag{14}$$

With z defined as: $z = \ln(\omega \cdot \tau_0) = \ln(\tau_0/\tau)$. Z_0 represents the dc-resistance, τ_0 is the characteristic time constant of the impedance function. The full impedance expression for the Zarc or (RQ) is:

$$Z_{(RQ)}(\omega) = \frac{1}{R^{-1} + \omega^\varphi Y_0 \cos\frac{n\pi}{2} + j\omega^\varphi Y_0 \sin\frac{n\pi}{2}} = R\frac{1 + (\omega\tau_0)^\varphi \cos\frac{n\pi}{2} - j(\omega\tau_0)^\varphi \sin\frac{\varphi\pi}{2}}{1 + 2(\omega\tau_0)^\varphi \cos\frac{\varphi\pi}{2} + (\omega\tau_0)^{2\varphi}} \tag{15}$$

The imaginary part of $Z_{(RQ)}$ then becomes:

$$Z_{(RQ),im.}(\omega) = R\frac{-\sin\frac{\varphi\pi}{2}}{\frac{1}{(\omega\tau_0)^\varphi} + 2\cos\frac{\varphi\pi}{2} + (\omega\tau_0)^\varphi} \tag{16}$$

Applying the Fuoss-Kirkwood method with $Q = (\omega \cdot \tau_0)^\varphi = (\tau_0/\tau)^\varphi$, $C = \cos(\varphi\pi/2)$, $S = \sin(\varphi\pi/2)$, $(\omega \cdot \tau_0)^\varphi$ transforms to (transformation indicated by $\rightarrow$):

$$(\omega \cdot \tau_0)^\varphi \rightarrow Q[C + jS] \tag{17}$$

$$Z_+(\tau_0/\tau) = \frac{S}{\frac{1}{Q(C+jS)} + 2C + Q(C+jS)} = \frac{SC\left[Q + 2 + \frac{1}{Q}\right] - jS^2\left[Q - \frac{1}{Q}\right]}{C^2\left[Q + 2 + \frac{1}{Q}\right]^2 + S^2\left[Q - \frac{1}{Q}\right]^2} \tag{18}$$

$Z_+(\tau_0/\tau)$ denotes the positive transform. The complex conjugate, $Z_-(\tau_0/\tau)$, yields the same function with an opposite sign for the imaginary part, which thus cancels out. This is not surprising as the distribution function should be a real valued function. Hence equation (18) can be reduced to:

$$R \cdot G(\tau) = \frac{R}{2\pi} \frac{2SC\left[Q + 2 + \frac{1}{Q}\right]}{C^2\left[Q + 2 + \frac{1}{Q}\right]^2 + S^2\left[Q - \frac{1}{Q}\right]^2} = \frac{R}{2\pi} \frac{\sin\varphi\pi}{\cosh\left[\varphi\ln\left(\frac{\tau_0}{\tau}\right)\right] + \cos\varphi\pi} \tag{19}$$

which results in the well-known distribution function for a (RQ)-circuit. It represents a symmetric, bell-shaped curve on the log(τ) axis, see figure 7. The area under the curve of $R \cdot G(\tau)$ equals R. The full width at half maximum (FWHM) depends strongly on the value of the exponent φ. In the case of $\varphi = 1/2$, i.e. representing a diffusion effect, the maximum drops significantly to $R \cdot (2\pi)^{-1} = 0.16\,R$, the FWHM then spans 2.33 decades. For φ close to 1 the curve becomes very narrow. With $\varphi = 0.95$ the maximum becomes $2.02\,R$ and the FWHM is 0.6 decade. Equation (19) turns into a δ-function for $\varphi = 1$, the (RQ) changes into a (RC) circuit with a single time constant, $\tau_0 = R \cdot C$.
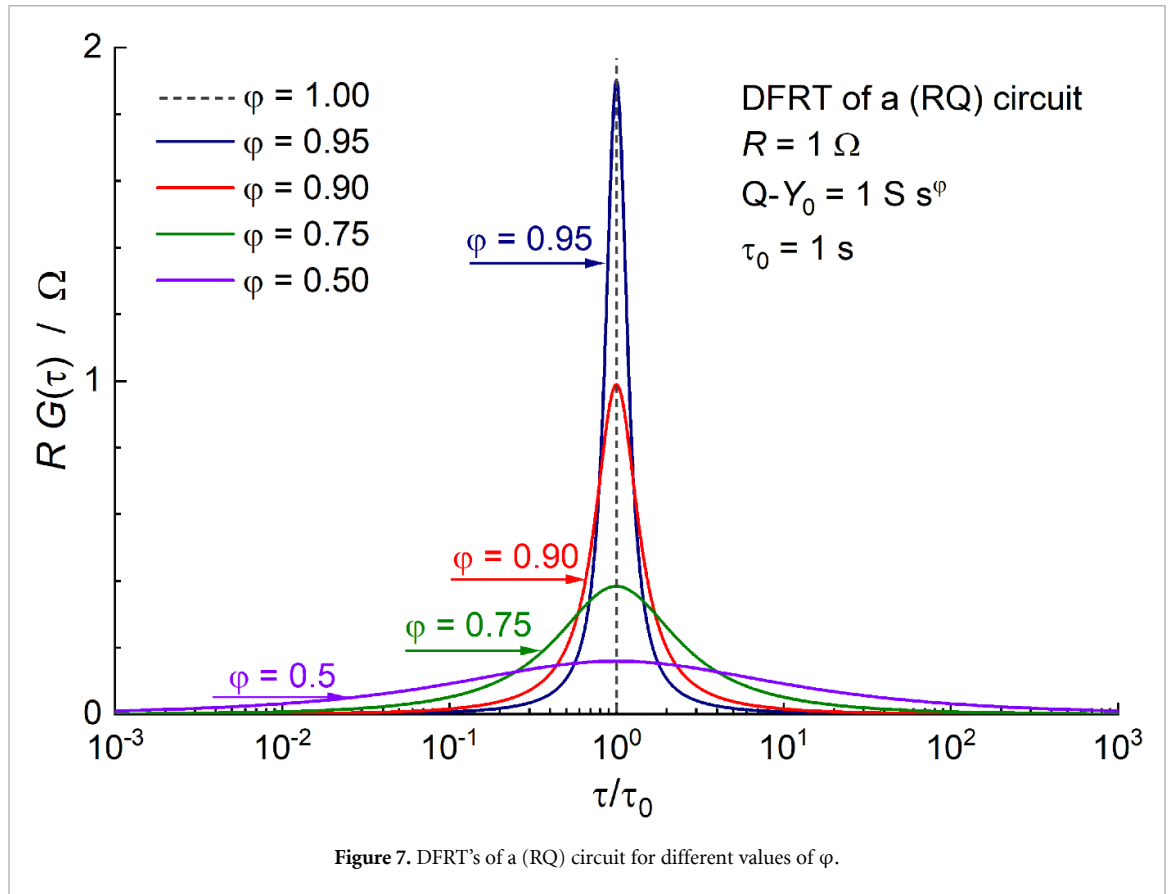
Figure 7. DFRT's of a (RQ) circuit for different values of φ.

3.1. Havriliak-Negami and Gerischer

The Havriliak-Negami dispersion [55, 56] has been postulated for the dielectric response of polymers:

$$\varepsilon(\omega) = \varepsilon_\infty + \frac{\varepsilon_0 - \varepsilon_\infty}{\left[1 + (j\omega\tau_0)^\beta\right]^\gamma} \tag{20}$$

For the impedance dispersion an analogues expression can be defined:

$$Z_{H-N}(\omega) = \frac{Z_0}{\left[1 + (j\omega\tau_0)^\beta\right]^\gamma} \tag{21}$$

For the special case of $\gamma = 1$, equation (21) represents the well-known Cole-Cole relation [57], i.e. the parallel combination of resistance and a CPE, i.e. a (RQ)-circuit or 'Zarc'. In the case that $\beta = 1$, the Cole-Davidson relation is obtained [58].

For a proper simulation of the H-N impedance equation (21) needs to be separated in a real and imaginary part:

$$Z_{H-N}(\omega) = \frac{Z_0}{\left[1 + (j\omega\tau_0)^\beta\right]^\gamma} = \frac{Z_0}{\left[1 + \cos\left(\frac{\beta\pi}{2}\right)(j\omega\tau_0)^\beta + j\sin\left(\frac{\beta\pi}{2}\right)(j\omega\tau_0)^\beta\right]^\gamma} = \frac{Z_0}{[a+jb]^\gamma} \tag{22}$$

With $a = 1 + \cos\left(\frac{\beta\pi}{2}\right)(j\omega\tau_0)^\beta$, $b = \sin\left(\frac{\beta\pi}{2}\right)(j\omega\tau_0)^\beta$, $(a+jb)^\gamma$ becomes:

$$(a+jb)^\gamma = \left\{\cos\left[\gamma \cdot \text{atan}\left(\frac{b}{a}\right)\right] + j\sin\left[\gamma \cdot \text{atan}\left(\frac{b}{a}\right)\right]\right\} (a^2 + b^2)^{\frac{\gamma}{2}} \tag{23}$$

Inserting in equation (22) and separating into a real and imaginary part leads to:

$$Z_{H-N}(\omega) = \frac{Z_0}{\left[1 + (j\omega\tau_0)^\beta\right]^\gamma} = Z_0 \frac{\cos\left[\gamma \cdot \text{atan}\left(\frac{b}{a}\right)\right] - j\sin\left[\gamma \cdot \text{atan}\left(\frac{b}{a}\right)\right]}{(a^2 + b^2)^{\frac{\gamma}{2}}} \tag{24}$$
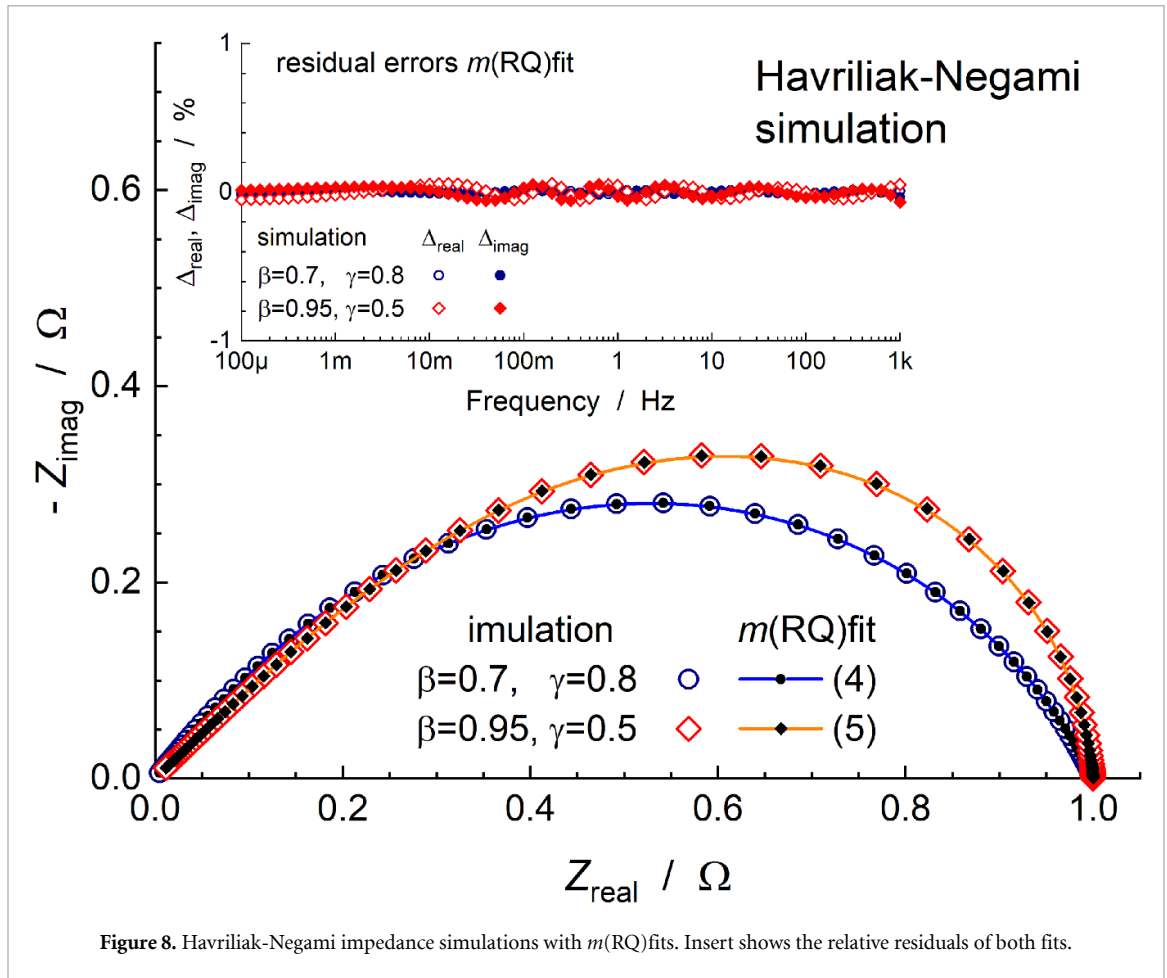
Figure 8. Havriliak-Negami impedance simulations with m(RQ)fits. Insert shows the relative residuals of both fits.

There are several publications with a derivation for the distribution function of the H-N type impedance [36, 59–61]. The equation presented by Macutkevic *et al* [36] seems to be incorrect. In the distribution function, presented by Bello *et al* [60, 61], a factor $(\tau/\tau_0)^{\beta\gamma}$ is missing. The correct version should read:

$$G(\tau) = \frac{1}{\pi}\left(\frac{\tau}{\tau_0}\right)^{\beta\gamma} \frac{\sin\left(\gamma\theta\right)}{\left[1 + 2\cos\left(\pi\beta\right)\left(\frac{\tau}{\tau_0}\right)^{\beta} + \left(\frac{\tau}{\tau_0}\right)^{2\beta}\right]^{\frac{\gamma}{2}}} , \text{ with : } \theta = \arctan\left(\frac{\sin\left(\pi\beta\right)}{\left(\frac{\tau}{\tau_0}\right)^{\beta} + \cos\left(\pi\beta\right)}\right) \quad (25)$$

A slightly different expression is published by Wan *et al* [44]. Examples of the H-N impedance ($Z_0 = 1\ \Omega$, $\tau_0 = 1$ s) with $\beta = 0.7$, $\gamma = 0.8$ and $\beta = 0.95$, $\gamma = 0.5$ are presented in figure 8. The m(RQ)fits to both dispersions are also shown, together with the relative residuals showing an excellent fit (<0.2%). The distribution functions present, depending on the values of β and γ more or less asymmetric peak shaped curves, see figure 9.

In figure 9 the m(RQ)fit, FT and Tikhonov DFRT's are shown in comparison with the exact DFRT, equation (25). Figure 9(a) shows that all three methods reproduce the major part of the distribution function quite well. With increasing value of β the distribution function becomes sharper and more asymmetric. Especially the m(RQ)fit cannot reproduce the exact DFRT properly, see figure 9(b), but the actual match to the simulated data for the 5(RQ)fit is excellent (relative deviations <0.2%). Both the FT and the Tikhonov inversions show some deviation from the ideal curve and a slight shift of the apparent τ_0.

3.2. Gerischer

A further increase in β to $\beta = 1$, results in an asymptotic shape for the DFRT, with $G(\tau) \to \infty$ for $\tau \to \tau_0$. $G(\tau)$ is nonexistent for $\tau > \tau_0$. The Gerischer impedance presents a special case of the Havriliak-Negami response, with $\beta = 1$ and $\gamma = 1/2$. The Gerischer dispersion represents semi-infinite diffusion combined with a side reaction of the mobile ion, see [62]. Despite the semi-infinite character, the impedance presents a
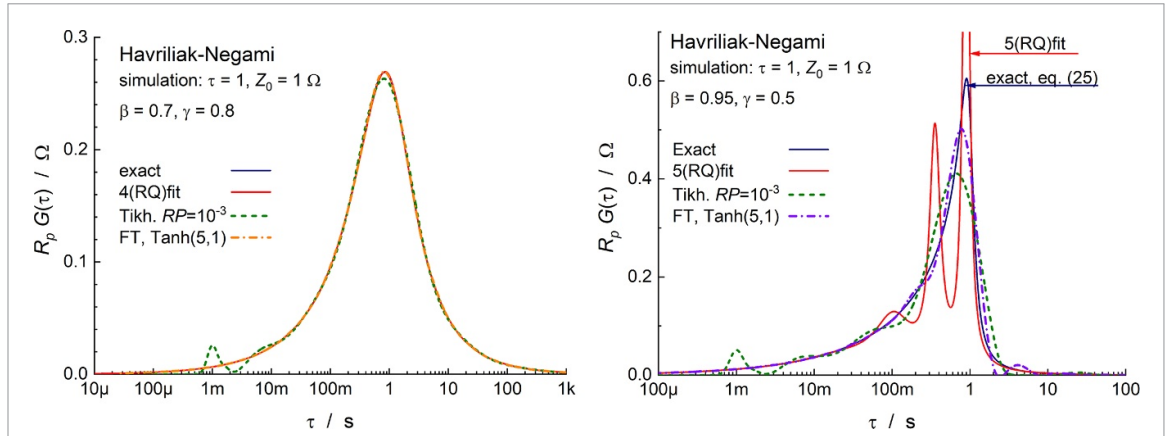
Figure 9. (a) DFRT for the H-N impedance with β = 0.7, γ = 0.8 and (b) with β = 0.95, γ = 0.5. All three inversion methods are presented with optimized parameter settings.
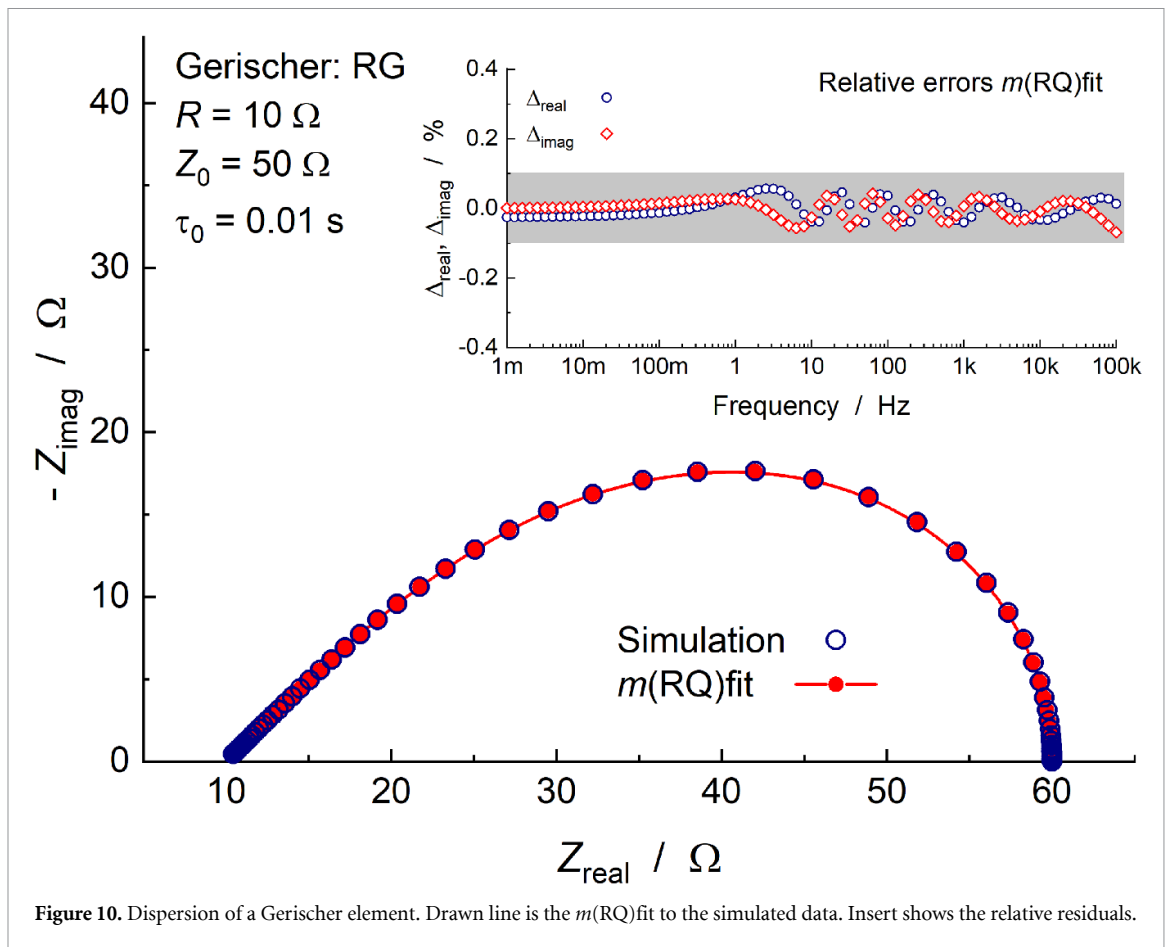

Figure 10. Dispersion of a Gerischer element. Drawn line is the m(RQ)fit to the simulated data. Insert shows the relative residuals.

dc-value. The general expression for the Gerischer (also known as a 'chemical impedance' [20, 21, 62]) reads:

$$Z_G(\omega) = \frac{Z_0}{\sqrt{1 + j\omega \cdot \tau_0}} = \frac{Z_0}{\sqrt{2}} \left[\sqrt{\frac{\sqrt{1 + \omega^2 \tau_0^2} + 1}{1 + \omega^2 \tau_0^2}} - j\sqrt{\frac{\sqrt{1 + \omega^2 \tau_0^2} - 1}{1 + \omega^2 \tau_0^2}} \right] \quad (26)$$

The impedance shows a Warburg dispersion (true semi-infinite diffusion presented by a line with 45° slope) in the high frequency region, which turns over to a (RC) type dispersion for $\omega \rightarrow 0$, see figure 10. The dispersion shown in figure 10 can be fitted with a series of five (RQ) circuits (of which two are capacitive) within the frequency range of 1 mHz–100 kHz. This m(RQ)fit shows a relative error of less than 0.1 %, see insert in figure 10, well within the range of the normal noise distribution.
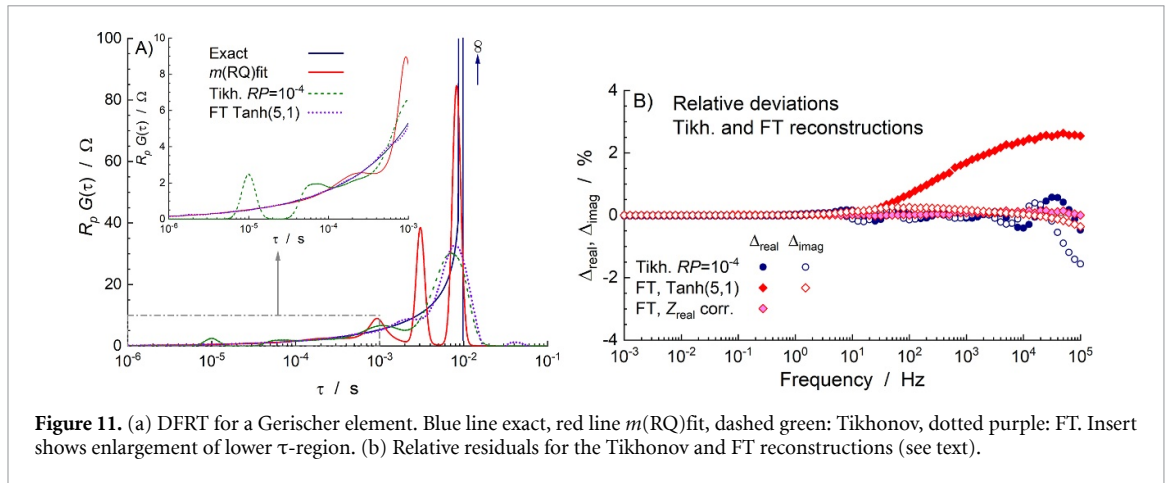
Figure 11. (a) DFRT for a Gerischer element. Blue line exact, red line m(RQ)fit, dashed green: Tikhonov, dotted purple: FT. Insert shows enlargement of lower τ-region. (b) Relative residuals for the Tikhonov and FT reconstructions (see text).

Inserting $\beta = 1$ and $\gamma = 1/2$ in equation (25) results in a simple expression for the Gerischer DFRT:

$$G_G(\tau) = \frac{1}{\pi}\sqrt{\frac{\tau}{\tau_0 - \tau}}, \tau \leq \tau_0 \wedge G_G(\tau) = 0, \tau > \tau_0 \tag{27}$$

The DFRT presents a simple asymptotic function, which is clearly related to the (RC) type behavior at low frequencies, which should yield a δ-function in τ-space. This presents a problem for the FT and Tikhonov inversions. Figure 11 shows the exact DFRT together with the m(RQ)fit, the FT inversion and the Tikhonov inversion. The last two show quite similar behavior with a broad main peak, while the m(RQ)fit shows two sharp peaks (two Gauss approximations).

The m(RQ)fit presents directly the reconstruction of the impedance, for the Tikhonov and FT reconstruction the DFRT is inserted in equation (1). It is quite remarkable that the m(RQ)fit shows a very good reconstruction with the average relative error of less than 0.1%, while the reconstructions for the Tikhonov and FT show in the high frequency range a significant deviation. The Δ_{real} for the FT show a large deviation, which is due to the use of only $Z_{im}(\omega)$ in the inversion, see equation (5). A small correction involving the true R_s and R_p values reduces this error significantly. The important point here is that the impedance reconstructions of the rather different DFRT's are all very close to the original data set. This shows that, at least for complex dispersions, different shapes are possible, hence the DFRT's are not necessarily unique.

3.3. Finite Length Warburg

The FLW presents the frequency dispersion for diffusion through a (thin) mixed conducting layer with the activity of the mobile ion fixed at one boundary. An example is the corrosion of iron with the formation of a $Fe(OH)_x$ layer. The exchange of Fe at the Fe/Fe(OH)x interface is much faster than the Fe^{2+} diffusion, thereby fixing the activity of the mobile ion at the Fe/Fe(OH)$_x$ interface. The general expression for the FLW is [63]:
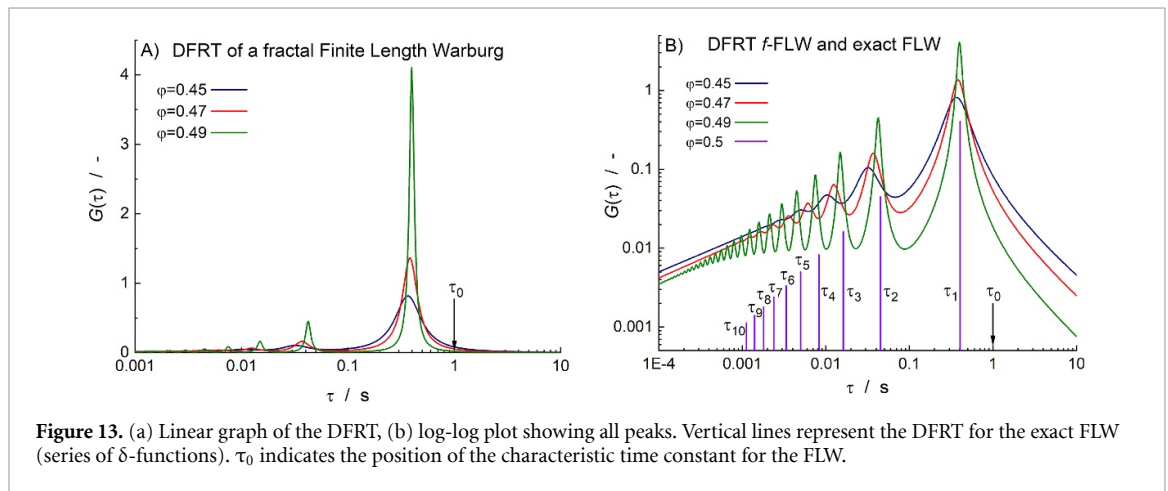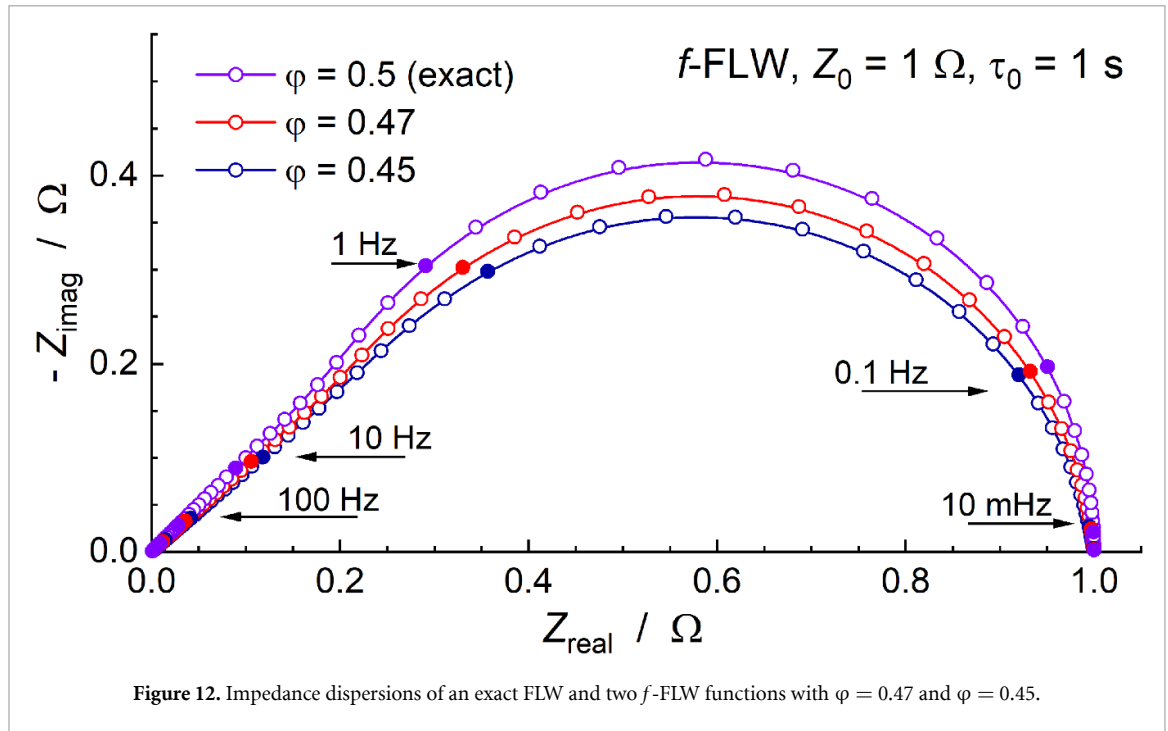
$$Z_{FLW}(\omega) = \frac{Z_0}{\sqrt{j\omega\tau_0}}\tanh\left(\sqrt{j\omega\tau_0}\right) = \frac{Z_0}{\sqrt{2\omega\tau_0}} \cdot \left[\frac{\sinh\sqrt{2\omega\tau_0} + \sin\sqrt{2\omega\tau_0}}{\cosh\sqrt{2\omega\tau_0} + \cos\sqrt{2\omega\tau_0}} - j\frac{\sinh\sqrt{2\omega\tau_0} - \sin\sqrt{2\omega\tau_0}}{\cosh\sqrt{2\omega\tau_0} + \cos\sqrt{2\omega\tau_0}}\right] \tag{28}$$

At high frequencies the FLW shows semi-infinite diffusion behavior (Warburg), which turns over to a capacitive (RC)-type response at low frequencies. The main difference between the FLW and the Gerischer dispersion is that the turnover to a low frequency (RC) starts with a small upturn above the 45° Warburg line, while the Gerischer shows a smooth transition to the low frequency (RC), see figure 5 in [29].

It is not possible to directly derive the DFRT for the FLW using the Fuoss-Kirkwood method [54]. With the 'fractal' form of the FLW [63, 64] the transformation to a DFRT is possible. The impedance expression for the f-FLW, $Z_{f\text{-FLW}}(\omega)$ with $\varphi < 0.5$, is given by:

$$Z_{f-\text{FLW}}(\omega) = \frac{Z_0}{(j\omega\tau_0)^\varphi}\tanh\left[(j\omega\tau_0)^\varphi\right] \tag{29}$$

Examples of the FLW and f-FLW are presented in figure 12. Using the representation in equation (29), the Fuoss-Kirkwood method can be applied, leading to the following expression in the τ-domain [63]:

Figure 12. Impedance dispersions of an exact FLW and two f-FLW functions with $\varphi = 0.47$ and $\varphi = 0.45$.

Figure 13. (a) Linear graph of the DFRT, (b) log-log plot showing all peaks. Vertical lines represent the DFRT for the exact FLW (series of δ-functions). τ_0 indicates the position of the characteristic time constant for the FLW.

$$G(\tau) = \frac{1}{\pi} \cdot \left(\frac{\tau}{\tau_0}\right)^{\varphi} \frac{\sin(\varphi\pi)\left(1 - Y^2\right) - 2\cos(\varphi\pi) \cdot Y \cdot \sin\left(2Q\sin(\varphi\pi)\right)}{1 + 2Y \cdot \cos\left(2Q\sin(\varphi\pi)\right) + Y^2} \tag{30}$$

with $Q = (\tau_0/\tau)^{\varphi}$ and $Y = \exp\left[-2Q\cos(\varphi\pi)\right]$.

Depending on the value of φ, several peak shapes appear in the DFRT, as can be seen in figure 13(a). For φ close to 0.5 many peaks appear. For $\varphi = 0.45$ approximately five peaks are seen in the log-log plot of figure 13(b). For $\tau \gg \tau_0$, equation (30) is simplified to [63]:

$$G(\tau) = \left(\frac{\tau_0}{\tau}\right)^{2\varphi} \frac{\sin(2\varphi\pi)}{3\pi} \tag{31}$$

In the limit $\tau \ll \tau_0$, equation (30) is reduced to [63]:

$$G(\tau) = \left(\frac{\tau}{\tau_0}\right)^{\varphi} \cdot \frac{\sin(\varphi\pi)}{\pi} \tag{32}$$
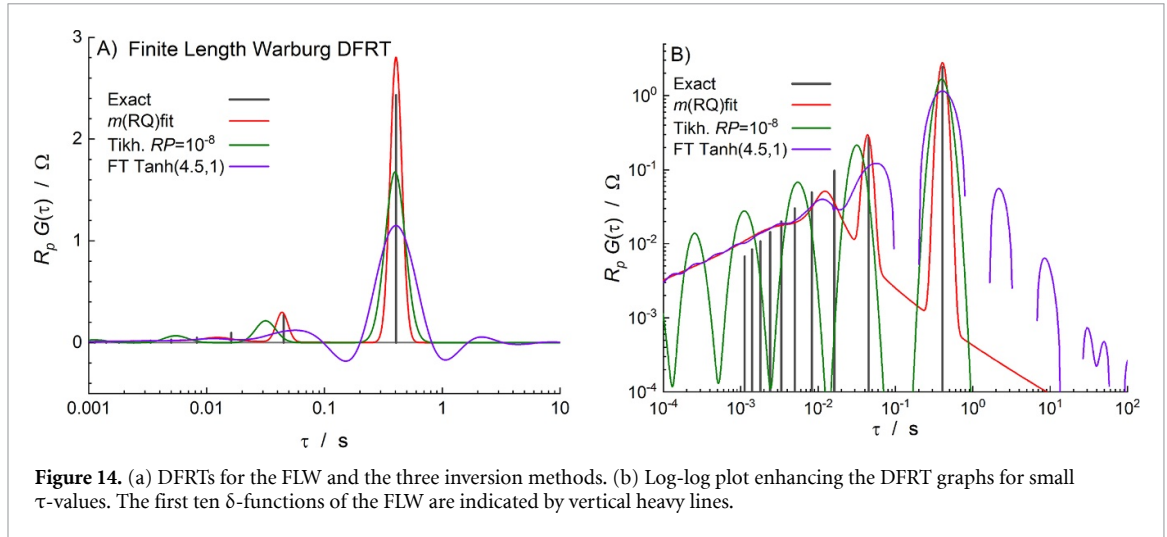
Figure 14. (a) DFRTs for the FLW and the three inversion methods. (b) Log-log plot enhancing the DFRT graphs for small τ-values. The first ten δ-functions of the FLW are indicated by vertical heavy lines.

In order to obtain the DFRT for an exact FLW, φ is replaced by $\varphi = 0.5 - \delta\,\pi^{-1}$. Taking the limit of equation (30) for $\delta \rightarrow 0$, results in an expression for the $G(\tau)$ of a FLW [63]:

$$G(\tau) = \frac{1}{\pi} \cdot \frac{2\delta + \left(2\delta^2 - \delta \cdot Q^{-1}\right) \cdot \sin(2Q)}{1 + (1 - 2Q\delta) \cdot \cos(2Q) - 2Q\delta} \tag{33}$$

For $\delta = 0$ the denominator of equation (33) reduces to: $Denom = 1 + \cos(2Q)$, which becomes zero for $Q = \pi\,(k\text{-}0.5)$, with $k = 1, 2, \ldots$. This results in a sum of δ-functions, for which the τ_k positions are given by:

$$\tau_k = \frac{\tau_0}{\pi^2 \cdot (k - 0.5)^2}, \; k = 1, 2, \ldots \tag{34}$$

The first major peak or δ-function occurs at $0.4053 \times \tau_0$, which is a rather unusual result. The corresponding impedance response for a δ-function is a (RC) circuit, Hence, based on the relation in equation (34), the dispersion of a FLW can be mimicked by an infinite series of (RC)'s, as was shown in [63].

$$Z_{FLW}(\omega) = Z_0 \sum_{k=1}^{\infty} 2\tau_k \frac{1 - j\omega\tau_k}{1 + \omega^2\tau_k^2} \tag{35}$$

The low frequency (RC)-type dispersion poses a problem for a proper inversion, as also observed for the DFRT of the Gerischer (figure 11). Figure 14(a) shows the m(RQ)fit (three (RQ)'s and two low frequency (RC)'s), the Tikhonov regularization with $RP = 10^{-8}$, and the FT-inversion with a Tanh(4.5,1) window. The first ten δ-functions are also presented by the heavy vertical lines. The heights present the relative values of the corresponding resistances, $R_k = 2\,Z_0 \cdot \tau_k$.

The m(RQ)fit presents the first two δ-functions quite well. The Tikhonov inversion with $RP = 10^{-8}$, shows many peaks as can be seen in the log-log plot of figure 14(b). increasing the RP to higher values decreases the number of peaks, which become wider as well. The FT-inversion is characterized by negative sections. These cannot be removed by narrowing the window down to Tanh(1,1), which results in a very shallow and broad peak. Because of the negative sections the FT-DFRT appears disrupted in the log-log plot of figure 14(b). Despite the rather different appearance of the DFRT's, the impedance reconstructions are very close to the original simulated data. The relative errors for the m(RQ)fit are less than 0.03% ($\chi^2_{CNLS} = 10^{-8}$). The relative residuals for the Tikhonov and the FT-inversion are presented in figure 15, these are all less than 0.5%, which is generally close to, or even less than the normal noise level in actual impedance data. Based on these results, it is clear that the appearance of the DFRT is not suited for judging the type of EqC or dispersion relations. It shows that several shapes of a DFRT can exist which, within the acceptable error margin, all fulfil equation (1).

4. Applications

4.1. SOFC electrodes
SOFC electrodes often present a rather featureless impedance, while it is clear that several processes in the electrode with different time constants contribute to the impedance. Figure 16 shows an example of the
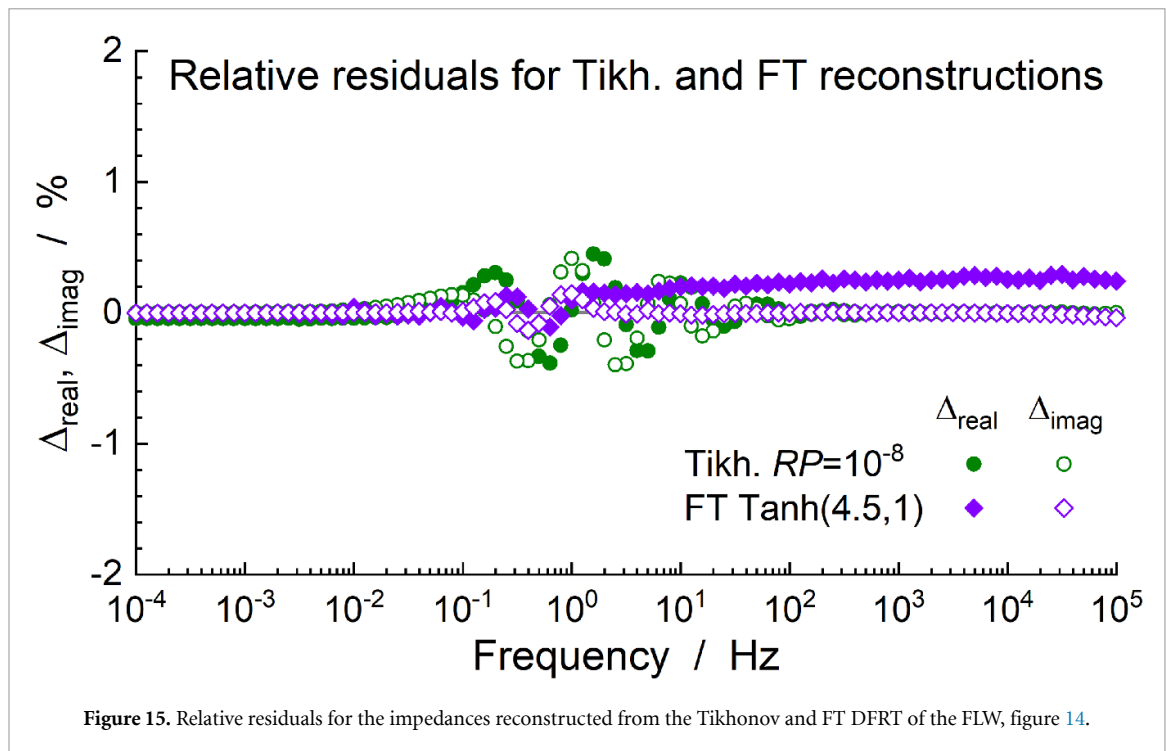
Figure 15. Relative residuals for the impedances reconstructed from the Tikhonov and FT DFRT of the FLW, figure 14.

impedance of a $Ca_3Co_4O_{9+\delta}$-$C_{0.9}Gd_{0.1}O_{1.95}$ (abbreviated: CCO/CGO 50/50) composite electrode for SOFC applications. This electrode was part of a set of compositions, ranging from 80% CCO–20% CGO to 30% CCO–70% CGO, see Rolle *et al* [65]. Measurements were performed in air over a temperature range from 600 °C to 850 °C. A first analysis of these rather featureless impedances was done with the m(RQ)fit. It should be stressed here that the DFRT did not give an indication of the presence of a Gerischer element. Based on these preliminary results an EqC could be formulated. The inclusion of a Gerischer dispersion was based on previous experience and literature reports for these types of cathodes, see [21, 22, 65, 66]. All impedances could be fitted to one single EqC, see the CDC in figure 16. A consistent model for all compositions and all temperatures was obtained [65]. Interestingly, the reaction rate K_a (or time constant, $\tau_G = K_a^{-1}$) for the Gerischer expression was virtually identical for all compositions. The Gerischer was tentatively contributed to surface oxygen adsorption/dissociation and diffusion on the CGO particles, hence related to a materials property and thus identical for all compositions. With the well-established EqC and circuit parameters an 'exact' DFRT can be constructed and compared with the three inversion methods.

This shows that the Gerischer contribution complicates the inversion to a DFRT, which is due to the low-frequency capacitive behavior, i.e. the presence of a limiting (RC) circuit. The m(RQ)fit can properly model a Gerischer dispersion, as was demonstrated in [29, 30], but the related DFRT showed several (sharp) peaks, see figure 11(a). The DFRT obtained with the m(RQ)fit for the impedance of figure 14 also shows an improper rendering of the Gerischer DFRT, as shown in figure 17(a). Two different circuits were used: RL-3(RQ)-(RC) and RL-3(RQ)-2(RC). The pseudo χ^2-values were 1.5×10^{-7} and 1.3×10^{-7} respectively. The last one is identical to the CNLS-fit with the Gerischer based EqC (see figure 16). The RL-3(RQ)-2(RC) model reproduces the low-frequency (RC) and the Gerischer asymptote quite accurately, but the two high-frequency (RQ) circuits (with a diffusive nature: $\varphi \approx 0.5$) are poorly reproduced.

Both the FT-inversion and the Tikhonov Regularization DFRT's show a poor performance in replicating the exact DFRT, see figure 17(b). The high-frequency (low-τ) peak in the Tikhonov DFRT can easily be misinterpreted as a real process, while it is obviously an artifact of the inversion procedure. For the major part, both the FT and Tikhonov are almost identical. The reconstructions of both the Tikhonov and FT inversion match quite well with the actual data. The Tikhonov reconstructions show a good match at low frequencies, but the error in the imaginary part increases rapidly (>1%) above ~3 kHz.

4.2. Electrode without possible EqC
It is not always possible to find an EqC that provides reliable parameters, in which case the presentation of a DFRT could be helpful. An example, presented in [29, 31], is a $La_{0.4}Sr_{0.6}Co_{0.2}Fe_{0.8}O_{3-\delta}$ (LSCF) electrode sintered at 1300 °C. The high temperature caused a high degree of sintering, resulting in low porosity and a large number of closed pores. A reliable (simple) EqC could not be found, but a m(RQ)fit was possible with

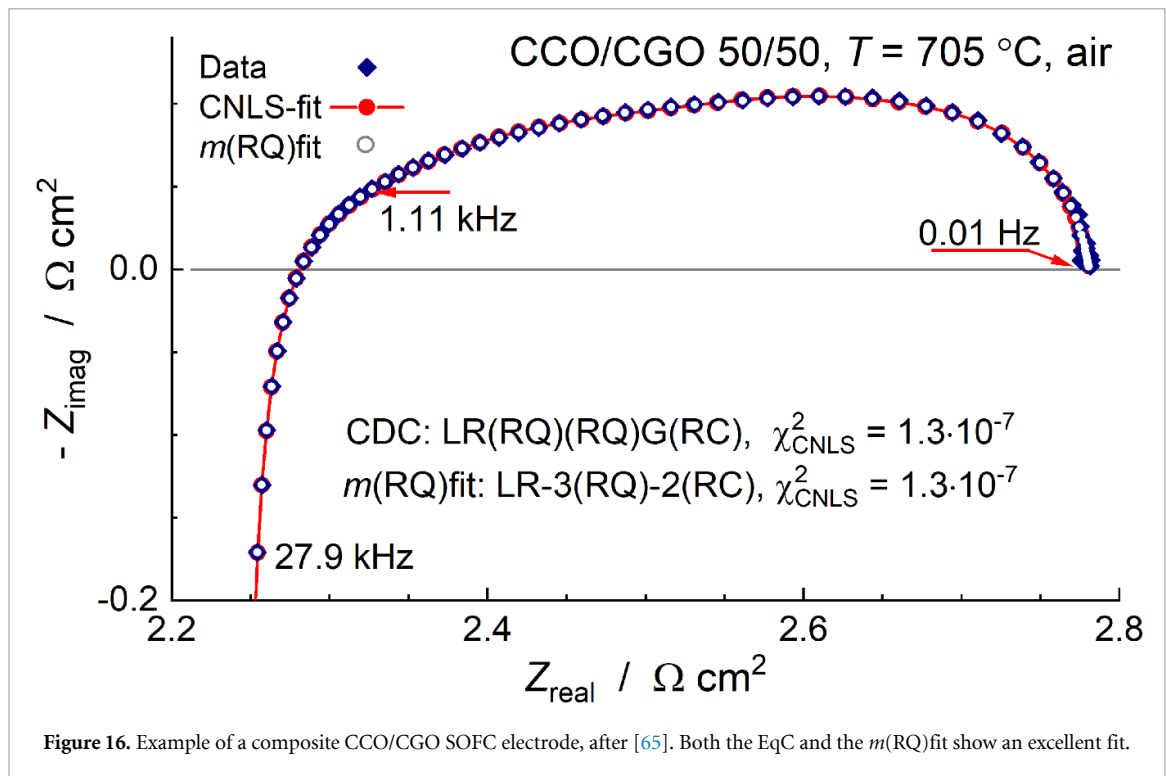**Figure 16.** Example of a composite CCO/CGO SOFC electrode, after [65]. Both the EqC and the *m*(RQ)fit show an excellent fit.
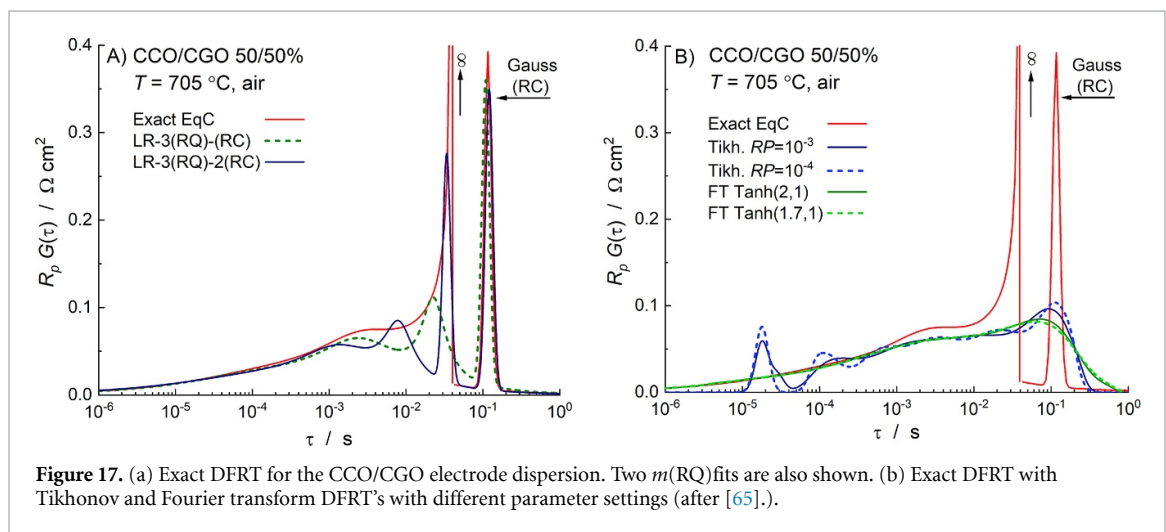

Figure 17. (a) Exact DFRT for the CCO/CGO electrode dispersion. Two *m*(RQ)fits are also shown. (b) Exact DFRT with Tikhonov and Fourier transform DFRT's with different parameter settings (after [65].).

six (RQ)'s. The relative errors in the parameters, however, vary from less than 1% to over 100%. The large values indicate strong correlation between the circuit parameters. Figure 18(a) presents the impedance at $T = 600\,°C$ and $pO_2 = 0.94$ atm. The *m*(RQ)fit presents two (RC)'s, see figure 18(b). This figure shows the DFRT's for three different pO_2-values. It shows that the major peak, a Gauss function for the (RC), is virtually independent of pO_2, while the broad peak shows a clear pO_2 dependence. The Tikhonov and Fourier inversions are not capable of rendering the capacitive nature of the major contribution, but the reconstructions, figure 18(a), are within reasonable bounds.

4.3. Battery research

Batteries, whether studied as single electrode in a three-electrode cell or as full battery cell or even as a battery stack, show diffusive/capacitive behavior at low frequencies, i.e. the absence of a dc-point. Within the standard frequency range down to, e.g. 10 mHz, this behavior appears as a sloping line in the low-frequency region, as depicted in figure 19(a). These types of impedances cannot be directly transformed to a DFRT. Schmidt *et al* [38] and Illig *et al* [67] have presented a method in which the low frequency tail is modelled with a simple EqC. Subsequently the diffusive/capacitive dispersion is subtracted from the original data. The remaining dispersion can then be transformed to a DFRT.
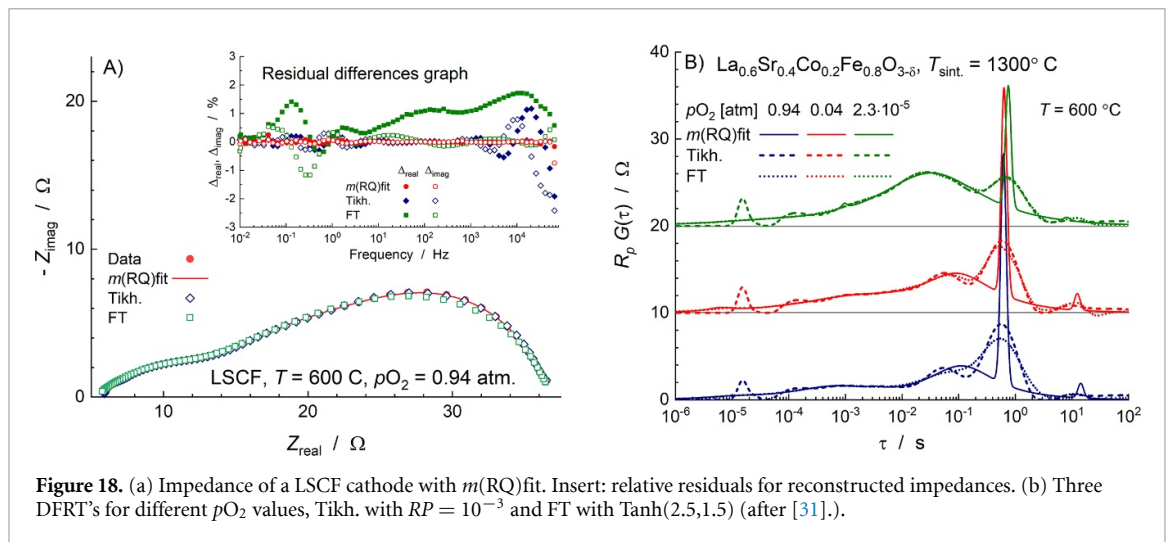
Figure 18. (a) Impedance of a LSCF cathode with $m(RQ)$fit. Insert: relative residuals for reconstructed impedances. (b) Three DFRT's for different pO_2 values, Tikh. with $RP = 10^{-3}$ and FT with Tanh(2.5,1.5) (after [31].).
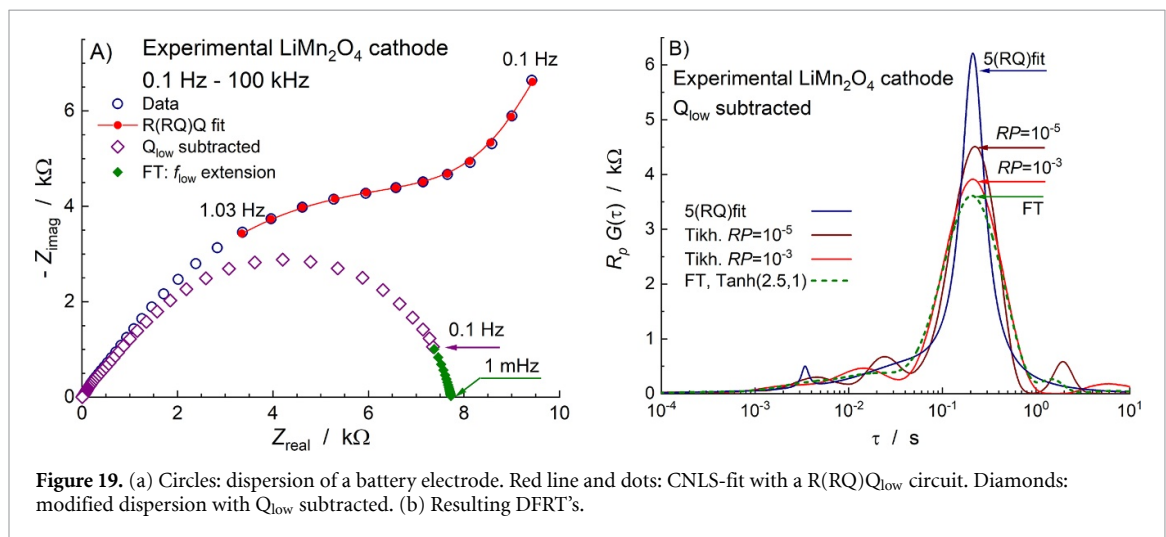

Figure 19. (a) Circles: dispersion of a battery electrode. Red line and dots: CNLS-fit with a $R(RQ)Q_{low}$ circuit. Diamonds: modified dispersion with Q_{low} subtracted. (b) Resulting DFRT's.

Here an example of this procedure is presented with the impedance of an experimental $LiMn_2O_4$ battery cathode, [68]. The low-frequency section could be modelled accurately with a partial CNLS-fit to a $R(RQ)Q_{low}$ circuit, see the red dots and line in figure 19(a). Subtracting the Q_{low} from the data set leads to an apparent dc-value. The resulting dispersion can then be used in the construction of a DFRT, as is shown in figure 19(b). The $m(RQ)$fit with five (RQ)'s shows a single large peak, with an asymmetric base. The Tikhonov inversion follows this curve quite well, but with some small fluctuations that show a dependence on the regularization parameter, RP. The FT-inversion, however, showed also a large negative peak for this modified data set. Extrapolation of the data set to lower frequencies, see green diamonds in figure 19(a), was needed to obtain an acceptable DFRT (dotted green line in figure 19(b)). All three inversion methods indicate a single major dispersion.

Impedance measurements are also an important tool in studying the aging and degradation of battery stacks, see e.g. Zhou *et al* [69]. With a conversion to a DFRT, the peak positions and peak heights can be monitored as a function of the State of Charge (SoC) and of the influence of cycling under various conditions. But again the diffusive/capacitive low-frequency branch needs to be removed. Figure 20 shows this subtraction procedure for a (unspecified) Li_xFePO_4 based battery stack under different SoC conditions. Figure 20(a) shows the stack impedance for a SoC of 20%, 50% and 80%. The low-frequency part was first fitted with a $R(RQ)Q_{low}$ circuit. The Q_{low} response was subtracted, together with the high-frequency inductive effect, resulting in the new dispersions of figure 20(b). Figure 21(a) shows the DFRT's obtained with the $m(RQ)$fit procedure with four (RQ)'s. Figure 21(b) presents the DFRT's obtained with Tikhonov Regularization ($RP = 10^{-3}$) and the FT-inversion with a Tanh(2.5,1) window. The $m(RQ)$fit shows very clearly four time constants, see table 1. The peak at $\tau = 0.21$ ms is a Gauss approximation of a δ-function, i.e. a (RC). The three smallest time constants are hardly affected by the SoC. Both the Tikhonov and FT inversions show less detail and wider peaks than the $m(RQ)$fit.

Table 1. Compilation of the time constants, obtained from the m(RQ)fit, at different states of charge. Bottom line: Tikhonov results from the Gauss curve deconvolution, figure 22.

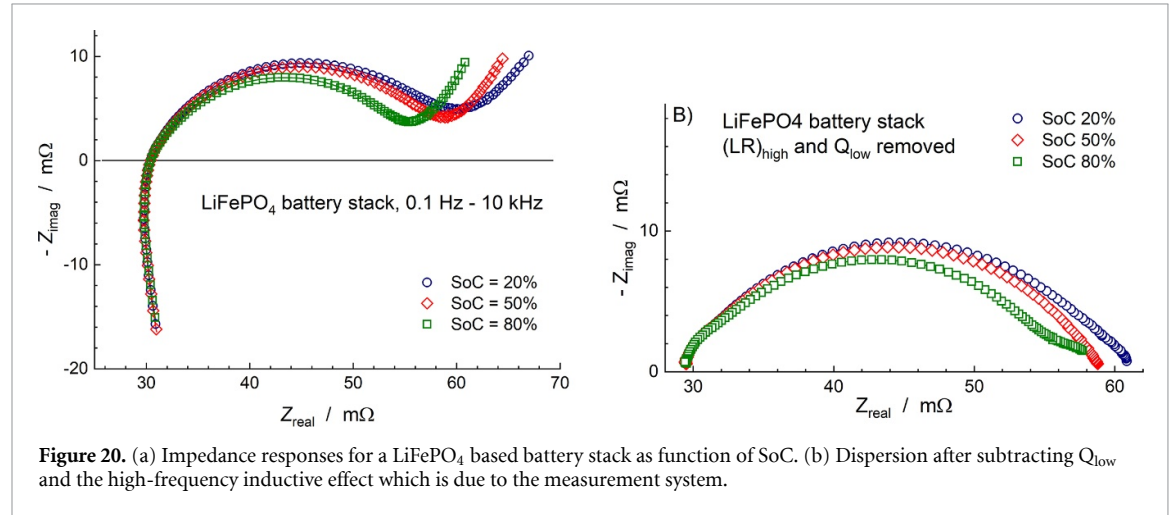| SoC	τ_A	τ_B	τ_C	τ_D	
20%	0.214	1.78	6.77	80	[ms]
50%	0.213	1.68	6.52	40	[ms]
80%	0.209	1.61	6.17	400	[ms]
Tikhonov:					
20%	0.195	2.30	7.79	61/300	[ms]

Figure 20. (a) Impedance responses for a LiFePO$_4$ based battery stack as function of SoC. (b) Dispersion after subtracting Q$_{low}$ and the high-frequency inductive effect which is due to the measurement system.
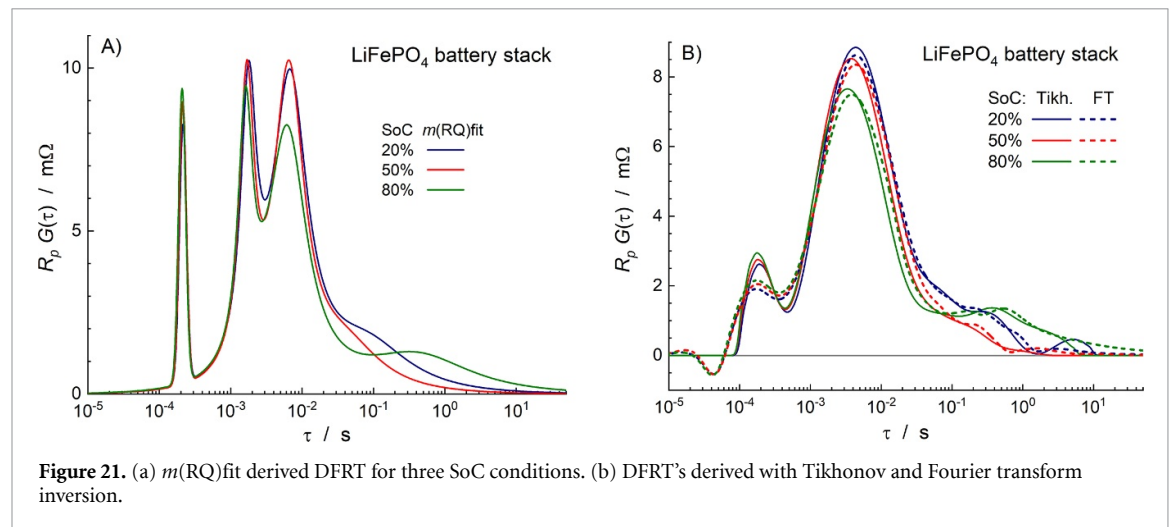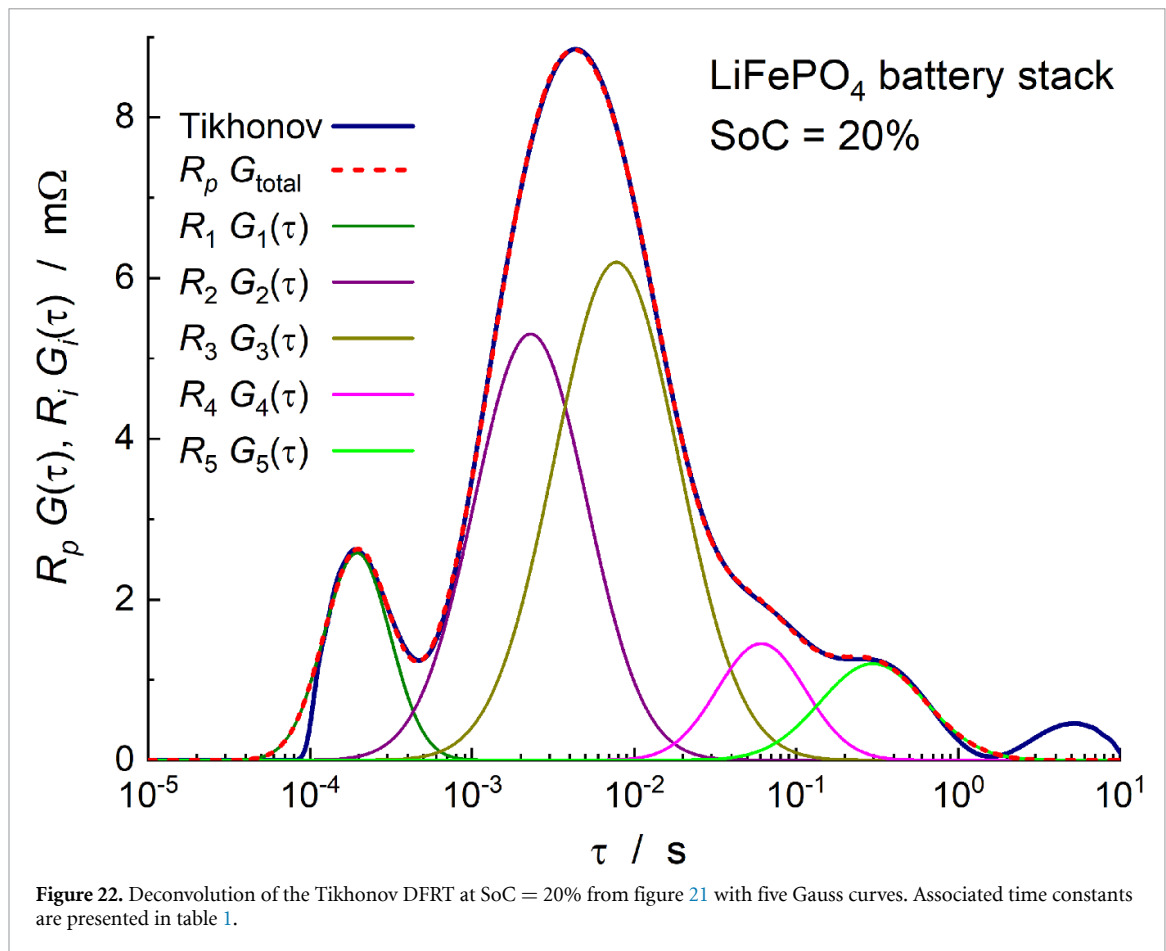

Figure 21. (a) m(RQ)fit derived DFRT for three SoC conditions. (b) DFRT's derived with Tikhonov and Fourier transform inversion.

Such a broad peak can consist of two Gauss curves. An attempt to deconvolute the Tikhonov DFRT at 20% SoC between $\tau = 0.1$ ms and $\tau = 1$ s is shown in figure 22. This τ-range could be fitted almost perfectly with five Gauss curves. The separate contributions and the overlapping envelope are presented. The three lowest time constants match reasonably well with the results from the m(RQ)fit. The low-frequency region ($\tau > 10$ ms) yields, however, two time constants. When a broad peak is present in the Tikhonov DFRT, it might be useful to consider deconvolution with a set of Gauss curves.

4.4. 'Inductive' effects

A special class of impedance problems is the appearance of a 'so-called' inductive effect in the impedance. Sometimes it is not apparent by visual inspection of the dispersion, but it will show up in a proper CNLS-analysis. The use of an inductor in the modelling is, however, incorrect. The negative contribution (in the '- Z_{imag}' representation) is the result of a ***negative differential*** resistance parallel to a ***negative differential*** capacitance (or CPE). This combination is not in violation with the Kramers-Kronig rules. Klotz has recently presented a review on this phenomena in [70]. Typical examples are SOFC/SOEC electrodes
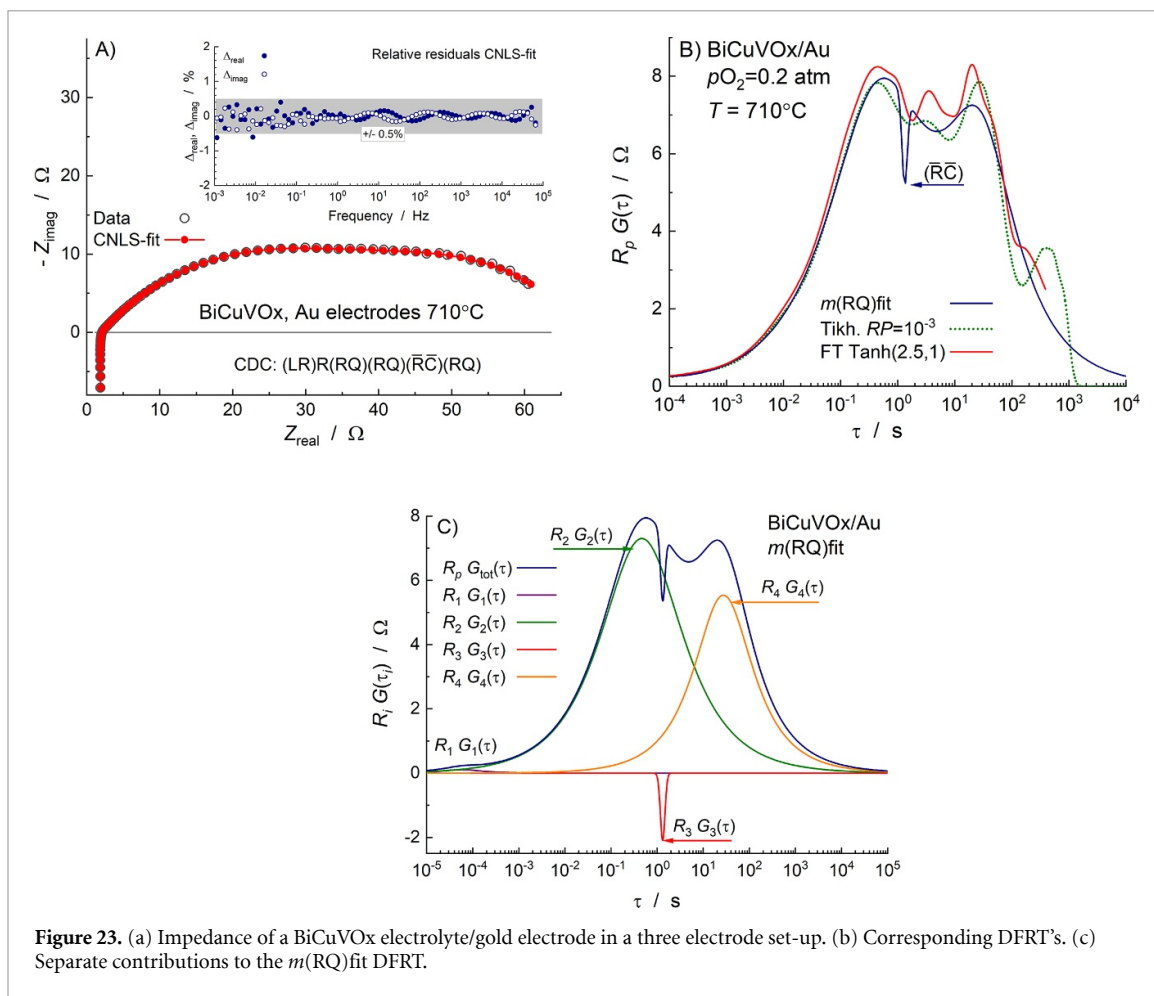
Figure 22. Deconvolution of the Tikhonov DFRT at SoC = 20% from figure 21 with five Gauss curves. Associated time constants are presented in table 1.

under bias. Van Hassel *et al* [71, 72] have provided a physical interpretation for the occurrence of a 'negative loop' in the impedance of a gold/air electrode under bias on a YSZ electrolyte. But the effect can also appear at zero bias in a three electrode set-up. This is often due to cross-talk between the reference and working electrodes, mediated through surface diffusion of oxygen species on an oxide conducting electrolyte [72–75] or caused by a mismatch between counter and working electrode, caused by a poorly performing counter electrode [76].

As an example the electrode response of a porous gold electrode on a $Bi_2Cu_{0.1}V_{0.9}O_{5.35}$ (BiCuVOx) electrolyte in a three-electrode set up is presented. The Pt-reference electrode is placed in the center of the annular work electrode. Figure 23(a) shows a typical impedance diagram with the CNLS-analysis and EqC, which comprises a negative (RC) circuit. The insert shows the relative residuals of the CNLS-fit.

Figure 23(b) shows the three DFRT's obtained with the inversion methods. Only the $m(RQ)$fit shows the negative (RC), presented by a Gauss curve. The four contributions to the overall $m(RQ)$fit DFRT are presented in figure 23(c). The Tikhonov inversion cannot present these 'inductive effects', the FT-method can show a negative distribution function when it is more pronounced (results not shown). But, as stated before, the $m(RQ)$ fit can result in unrealistic negative contributions. In this case, however, careful analysis with the partial fit and subtraction method [74], showed consistently the presence of a negative (RC) contribution for all temperatures and oxygen partial pressures. This was then assigned to a cross talk between reference and work electrode through surface diffusion of (charged?) oxygen species [74–76]. The above clearly shows that unexpected contributions to the overall dispersion can go unnoticed in the transformation to a DFRT.

5. Discussion

The growing number of publications on development and application of a procedure for a DFRT shows that it has become a well-established tool in the analysis of impedance data. Hence, it is justified to take a critical look at the advantages and limitations of this procedure. Most importantly, it should be an easy to apply method for the general scientist. The freely available 'DRTtools' MatLab® program published by Dr. Wan has this property [44, 47]. The FT method presented here requires extra steps for the extension of the frequency range. The FFT inversion presented by Schichlein *et al* [27] is in principle a single step procedure in which

Figure 23. (a) Impedance of a BiCuVOx electrolyte/gold electrode in a three electrode set-up. (b) Corresponding DFRT's. (c) Separate contributions to the m(RQ)fit DFRT.

only the Hann-window setting needs to be adjusted. But both these FT-methods use only the imaginary part of the impedance data. A Kramers-Kronig data validation is essential in that case.

The newly developed m(RQ)fit is not simple to execute, as it takes a number of successive steps in order to approach the optimum fit. The clear advantage is that it produces sharp peaks and it shows clearly capacitive effects in the impedance. But the presence of a Gerischer can cause parasitic peaks [29], making interpretation more complex. The FLW is also problematic for the regular inversion methods, but here the m(RQ)fit seems to reproduce the first two peaks quite well, see figure 14. A major drawback of the m(RQ)fit is that an acceptable fit to the impedance data is not always guaranteed, an unwanted negative (RQ) can appear. Hence, it is no surprise that Tikhonov Regularization is currently the most used inversion method.

The DFRT is presented as a model free approach, as opposed to the EqC based CNLS-analysis. Model free is, however, a contradiction as it is assumed that all time constants, and hence the electrochemical processes, can be arranged in series. This is, of course, a (quite simple) model in itself. When an EqC can be found with a good fit to the data, i.e. with a relative differences distribution, e.g. equation (11), close to that obtained from the Kramers-Kronig data validation [9, 26, 27], then the EqC provides a plausible description of the electrochemical processes. That is, provided that physical meaning can be assigned to the EqC. For a linear arrangement of sub-circuits, e.g. (RQ)'s, and dispersive elements (Gerischer, FLW), the 'exact' DFRT can be directly derived, as was shown for the CCO/CGO cathodes [65]. Of course, the EqC in this case is also an approximation of the highly distributed electrochemical processes in the porous composite CCO/CGO cathode. Comparison with the DFRT's obtained through the inversion methods shows sometimes significant deviations, although the impedance reconstructions match reasonably well with the original data.

A key point in obtaining an optimal DFRT is high quality impedance data. That is, over as large a frequency range as possible, with minimal noise and sufficient points per decade (ppd). Zang *et al* [45] have shown that increasing the ppd to 100 or even 1000 improves the quality of the DFRT. For the Tikhonov inversion, stray data points (e.g. close to 50 or 60 Hz) and clear outliers should not be removed, but rather replaced by data points obtained by interpolation between adjacent data sets (see figure 6 in [31]).

A new development in improving the quality of the Tikhonov based inversions is the use of an adaptive regularization parameter, which is also a function of τ: $\lambda(\tau)$. Using information from the differences between

the measured and reconstructed impedance, the shape of $\lambda(\tau)$ is optimized. Zhang *et al* [46] have shown that using this method a quite reasonable rendering of the DFRT of a Gerischer could be obtained. Žic *et al* [77] have also presented an adaptive Tikhonov inversion method based on a collocation procedure.

The question of reliability depends on what results are expected from the obtained DFRT. A global presentation of relaxation times, i.e. peaks, is simple. But deriving a possible overall impedance model for the electrochemical device is often not possible. With all three presented inversion methods the presence of special diffusion processes (Gerischer, FLW) cannot be identified from the DFRT. With the Tikhonov inversion one should be aware that rather broad peaks may contain two time constants. De-convolution with a set of Gauss curves can increase the resolution between time constants, as was shown for the Li_xFePO_4 based battery stack (figure 22).

More importantly, small but significant contributions to the overall dispersion can go unnoticed in the DFRT. The analysis of the BiCuVOx impedance showed that the minor negative (RQ) contribution is not recognized by the Tikhonov inversion. The FT-DFRT showed only a hint (dip between peaks in figure 23(b)). Only the m(RQ)fit, which was identical to the CNLS derived EqC, was able to show the negative contribution. In a previous publication [29] the DFRT was calculated for a mixed conducting lead-zirconate-titanate (PZT) relaxor [10, 78]. CNLS-analysis showed besides a large electronic conductivity also a minor, but significant, ionic conductivity to be present. The dispersion related to the ionic conductivity could not be observed in the DFRT, showing that the CNLS-analysis has an advantage in this case. Furthermore, the presence of a diffusion related dispersion, i.e. the parallel combination of a Warburg and resistance, (RQ) with $\varphi = 1/2$, results in a shallow peak that spans several decades. In combination with strong peaks it may also go unnoticed in the DFRT.

The discussions above and in the previous sections show that one cannot be certain that the DFRT shows all dispersive processes. A combination of τ-domain (DFRT) and frequency domain (CNLS) analysis, as presented by Sonn *et al* [37], presents a more secure tool for impedance data analysis. When a trustworthy EqC can be obtained from the CNLS-analysis, i.e. relative residuals for CNLS and KK-data validation show a good match, then the added value of a DFRT is the graphical representation of the various time constants and peak shapes. The bottom line, however, remains that solving the Fredholm integral, equation (1), is and will be an 'ill-posed inverse problem'.

6. Conclusions

- Deriving a DFRT is a good way of showing the dispersive processes in an electrochemical devise. These are characterized by peaks positioned at the characteristic time constants. But one should realize that these DFRTs are not necessarily unique. Different distributions can produce reconstructed impedances that are quite close to the original data (almost within the experimental error distribution).
- The Gerischer and FLW dispersions pose problems with the straightforward inversion programs, resulting in an incorrect rendering of the exact DFRT.
- The m(RQ)fit method produces sharper peaks, but is prone to satellite peaks when a Gerischer dispersion is present. Sometimes this method can produce an unwanted negative (RQ) contribution.
- With the basic Tikhonov inversion, broad peaks should be tested for extra contributions.
- A combination of inversion to a DFRT and CNLS-analysis is recommended. Comparing the impedance, reconstructed from the DFRT, with the original data is an important validation step.

Acknowledgments

ORCID iD

Bernard A Boukamp ⓘ https://orcid.org/0000-0001-7348-5385

References

[1] Sluyters-Rehbach M and Sluyters J H 1970 *Electroanalytical Chemistry* vol 4, ed A J Bard (New York: Marcel Dekker) pp 1–127
[2] Sluyters-Rehbach M and Sluyters J H 1984 *Comprehensive Treatise of Electrochemistry* vol 9, ed E Yaeger, J O M Bockris, B E Conway and S Sarangapini (New York: Plenum) pp 177

[3] Wapenaar K E D and Schoonman J 1981 *Solid State Ion.* **5** 637–40

[4] Macdonald J R and Potter Jr L D 1987 *Solid State Ion.* **24** 61–79

[5] Boukamp B A 1986 *Solid State Ion.* **20** 31–44

[6] Boukamp B A 1986 *Solid State Ion.* **18–19** 136–40

[7] Dygas J R, Fafilek G, Durakpasa H and Breiter M W 1993 *J. Appl. Electrochem.* **23** 553–8

[8] Wisse A and Boukamp B A EqCwin95 (available at: www.wisseq.nl/portfolio.aspx) (in Dutch)

[9] Boukamp B A 2004 *Solid State Ion.* **169** 65–73

[10] Boukamp B A and Blank D H A 2011 *IEEE-TUFFC* **58** 2521–30

[11] Barsoukov E and Macdonald J R eds 2005 *Impedance Spectroscopy: Theory, Experiment, and Applications* 2nd edn (New York: Wiley)

[12] Orazem M E and Tribollet B 2008 *Electrochemical Impedance Spectroscopy* (New York: Wiley)

[13] Lvovich V F 2012 *Impedance Spectroscopy. Applications to Electrochemical and Dielectric Phenomena* (New York: Wiley)

[14] Lasia A 2014 *Electrochemical Impedance Spectroscopy and Its Applications* (Berlin: Springer)

[15] Fletcher S 1994 *J. Electrochem. Soc.* **141** 1823–6

[16] Zview, Scribner Associates ZView® For Windows (available at: www.scribner.com/software/68-general-electrochemistr376-zview-for-windows/)

[17] Rolle A, Thoréton V, Rozier P, Capoen E, Mentré O, Boukamp B and Daviero-Minaud S 2012 *Fuel Cells* **12** 288–301

[18] Wilson J R, Kobsiriphat W, Mendoza R, Chen H-Y, Hiller J M, Miller D J, Thornton K, Voorhees P W, Adler S B and Barnett S A 2006 *Nat. Mater.* **5** 541–4

[19] Wilson J R *et al* 2007 *ECS Trans.* **7** 1879–87

[20] Almar L, Szász J, Weber A and Ivers-Tiffée E 2017 *J. Electrochem. Soc.* **164** F289–F97

[21] Adler S B, Lane J A and Steele B C H 1996 *J. Electrochem. Soc.* **143** 3554–64

[22] Lu Y, Kreller C and Adler S B 2009 *J. Electrochem. Soc.* **156** B513–B25

[23] Franklin A J and De Bruin H J 1983 *Phys. Status Solidi* a **75** 647–56

[24] Boukamp B A CDC_Explained.pdf (available at: https://www.utwente.nl/en/tnw/ims/downloads/)

[25] Brug G J, van den Eeden A L G, Suyters-Rehbach M and Sluyters J H 1984 *J. Electroanal. Chem.* **176** 275–95

[26] Boukamp B A 1995 *J. Electrochem. Soc.* **142** 1885–94

[27] Schichlein H, Müller A C, Voigts M, Krügel A and Ivers-Tiffée E 2002 *J. Appl. Electrochem.* **32** 875–82

[28] Sonn V, Leonide A, Weber A and Ivers-Tiffée E 2008 *J. Electrochem. Soc.* **155** B36–B41

[29] Boukamp B A 2015 *Electrochim. Acta* **154** 35–46

[30] Boukamp B A and Rolle A 2017 *Solid State Ion.* **302** 12–18

[31] Boukamp B A and Rolle A 2018 *Solid State Ion.* **314** 103–11

[32] Hansen P C 1994 *Numer. Algorithms* **6** 1

[33] DTU Compute (www.imm.dtu.dk/~pcha/Regutools/)

[34] Regtools version 1.1.0.0 MathWorks (www.mathworks.com/matlabcentral/fileexchange/52-regtools)

[35] Dion F and Lasia A 1999 *J. Electroanal. Chem.* **475** 28

[36] Macutkevic J, Banys J and Matulis A 2004 *Nonlinear Anal. Model. Control* **9** 75–88

[37] Sonn V, Leonide A and Ivers-Tiffée E 2008 *J. Electrochem. Soc.* **155** B675–B79

[38] Schmidt J P, Chrobak T, Ender M, Illig J, Klotz D and Ivers-Tiffée E 2011 *J. Power Sources* **196** 5342–8

[39] Sumi H, Yamaguchi T, Hamamoto K, Suzuki T, Fujishiro Y, Matsui T and Eguchi K 2012 *Electrochim. Acta* **67** 159–65

[40] Illig J, Schmidt J P, Weiss M, Weber A and Ivers-Tiffée E 2013 *J. Power Sources* **239** 670–9

[41] Ramos T, Søgaard M and Mogensen M B 2014 *J. Electrochem. Soc.* **161** F434–F44

[42] Kazlauskas S, Kežionis A, Šalkus T and Orliukas A F 2013 *Solid State Ion.* **231** 37–42

[43] Saccoccio M, Wan T H, Chen C and Ciucci F 2014 *Electrochim. Acta* **147** 470–82

[44] Wan T H, Saccoccio M, Chen C and Ciucci F 2015 *Electrochim. Acta* **184** 483–99

[45] Zhang Y, Chen Y, Yan M and Chen F 2015 *J. Power Sources* **283** 464–77

[46] Zhang Y, Chen Y, Li M, Yan M, Ni M and Xia C 2016 *J. Power Sources* **308** 1–6

[47] DRTtools and manual (available at: https://sites.google.com/site/drttools/)

[48] Hörlin T 1993 *Solid State Ion.* **67** 85–96

[49] Hörlin T 1998 *Solid State Ion.* **107** 241–53

[50] Hershkovitz S, Baltianski S and Tsur Y 2011 *Solid State Ion.* **188** 104–9

[51] Drach Z, Hershkovitz S, Ferrero D, Leone P, Lanzini A, Santarelli M and Tsur Y 2016 *Solid State Ion.* **288** 307–10

[52] Oz A, Singh K, Gelman D, Thangadurai V and Tsur Y 2018 *J. Phys. Chem.* C **27** 15097–107

[53] Paul T and Tsur Y 2018 *Solid State Ion.* **323** 37–43

[54] Fuoss R M and Kirkwood J G 1941 *J. Am. Chem. Soc.* **63** 385–94

[55] Havriliak S and Negami S 1967 *Polymer* **8** 161–210

[56] Havriliak S and Havriliak S J 1996 *Polymer* **37** 4107–10

[57] Cole K S and Cole R H 1941 *J. Chem. Phys.* **9** 341–51

[58] Davidson D W and Cole R H 1951 *J. Chem. Phys.* **19** 1484–90

[59] Alvarez F, Alegra A and Colmenero J 1991 *Phys. Rev.* B **44** 7306–12

[60] Bello A, Laredo E and Grimau M 1999 *Phys. Rev.* B **60** 12764–74

[61] Bello A, Laredo E and Grimau M 2000 *J. Chem. Phys.* **113** 863–8

[62] Boukamp B A and Bouwmeester H J 2003 *Solid State Ion.* **157** 29–33

[63] Boukamp B 2017 *Electrochim. Acta* **252** 154–63

[64] Stoynov Z 1990 *Electrochim. Acta* **35** 1493–9

[65] Rolle A, Mohamed H A A, Huo D, Capoen E, Mentré O, Vannier R-N, Daviero-Minaud S and Boukamp B A 2016 *Solid State Ion.* **294** 21–30

[66] Hildenbrand N, Nammensma P, Blank D H A, Bouwmeester H J M and Boukamp B A 2013 *J. Power Sources* **238** 442–53

[67] Illig J, Ender M, Chrobak T, Schmidt J P, Klotz D and Ivers-Tiffee E 2012 *J. Electrochem. Soc.* **159** A952–A60

[68] Hendriks T A, Monteiro Cunha D, Singh D P and Huijben M 2018 *ACS Appl. Energy Mater.* **1** 7046–51

[69] Zhou X, Pan Z, Han X, Lu L and Minggao O 2019 *J. Power Sources* **417** 188–92

[70] Klotz D 2019 *Electrochem. Commun.* **98** 58–62

[71] van Hassel B A, Boukamp B A and Burggraaf A J 1991 *Solid State Ion.* **48** 139–54

[72] van Hassel B A, Boukamp B A and Burggraaf A J 1991 *Solid State Ion.* **48** 155–71

[73] Boukamp B A 2000 *ACH-Models Chem.* **137** 225–42
[74] Boukamp B A 2000 *Solid State Ion.* **135–137** 75–82
[75] Boukamp B A 2001 *Solid State Ion.* **143** 47–55
[76] Boukamp B A, Hildenbrand N, Nammensma P and Blank D H A 2011 *Solid State Ion.* **192** 404–8
[77] Žic M, Pereverzyev Jr S, Subotić V and Pereverzyev S 2020 *Int. J. Geomath.* **11** 2
[78] Boukamp B A, Pham M T N, Blank D H A and Bouwmeester H J M 2004 *Solid State Ion.* **170** 239–54